PROBABILISTIC CHARACTERIZATION OF EPOXI ADHESIVES

André Cardoso Martinho

Master's Thesis

Supervisor at FEUP: Dr. Abílio M. P. De Jesus
Co-supervisor at FEUP: Dr. José A.F. Oliveira Correia
Supervisors at UniOvi: Dra. María Jesus Lamela Rey
Dr. Alfonso Fernández-Canteli

Mestrado Integrado em Engenharia Mecânica

February 2018

Para a Alzira, o Hêrnani
e a Joana

Caracterização probabilística de adesivos epóxi

Resumo

Uma metodologia de caracterização probabilística de ruptura, usando o Generalized Local Model (GLM) (Calvente 2017) foi experimentada numa resina epóxi disponível comercialmente – EPOLAM 2025. O GLM foi aplicado a valores experimentais obtidos em ensaios de tração para provetes em forma de osso e em provetes *compact tension*, onde a tensão de ruptura foi considerada como parâmetro generalizado. Antes, foi realizada uma caracterização viscoelástica para analisar as propriedades do material, através de ensaios de relaxação a diferentes temperaturas. Foi aplicado o princípio de sobreposição temperatura-tempo aos ensaios realizados, obteve-se uma curva mestra para o módulo de relaxação e aproximou-se a curva com séries de Prony.

O material foi considerado estável e com um comportamento similar a linear elástico até 30°C, esta consideração foi corroborada pela curva tensão-deformação obtida nos ensaios de tração em provetes em forma de osso. É observada uma elevada dispersão dos valores da tensão de cedência, o que conduziu a uma aproximação a estes valores através de uma função de distribuição cumulativa de Weibull, com três paramêtros, que não é ideal. Uma função de distribuição cumulativa primária (PFCDF, segundo o GLM) foi obtida como propriedade relativa do material para $1mm^3$ mas a aplicabilidade desta função a outra geometria não foi validada com sucesso. Os modelos numéricos foram postos em causa e foram descobertas imprecisões mas sem soluções alternativas dentro do tempo estipulado para este projeto.

PROBABILISTIC CHARACTERIZATION OF EPOXI ADHESIVES

Abstract

A probabilistic characterization of failure, using the Generalized Local Model (GLM) (Calvente 2017), was attempted in a commercially available epoxy resin – EPOLAM 2025. The GLM was applied to experimental data from dogbone and compact tension specimens, considering the ultimate tensile strength as a generalized parameter. A prior viscoelastic characterisation was performed to analyse the material's behaviour, through relaxation tests at different temperatures. The temperature-time superposition principle was applied to these tests, a master curve for the relaxation modulus was obtained and the curve was approached using Prony series.

The material was found stable and with a behaviour close to linear elastic up to 30°C, this consideration was reassured by the outcome stress-strain curves of tensile tests in dogbone specimens. A high scatter in the ultimate tensile strength values was observed, which led to a non-ideal fit of the three-parameter Weibull cumulative distribution function to these values. A primary failure cumulative distribution function was obtained as a relative material property for $1mm^3$ but the applicability of this function to another geometry was not successfully validated. The numerical model was questioned and found imprecise but no alternative solution was found within the stipulated time for this project.

Acknowledgements

I wish to thank the EPIG team for guiding me throughout this project, in particular to Miguel Calvente and Pelayo Fernandez, for sharing with me their endless knowledge, for their guidance and for their availability. Also, would like to thank John McKenna, with whom I shared part of this project and helped me with his critic viewpoints, fruitful conversations and companionship.

The opportunity to develop this dissertation would not exist if it wasn't for Professor Dr. Abílio de Jesus, to who I am truly grateful.

I met outstanding people throughout my stay at FEUP and am proud of having shared full days and sometimes full nights with them, in this quest of becoming engineers. Some of them taught me to be more of a person as well and I would like to thank in particular to Joel Medeiros, Pedro Paixoto, Leonildo Leite, Carlos Pereira and Estela Bento, as they truly inspire me and made this journey more pleasant. Also would like to thank my Gijón's flatmates, Susana, Federica, Meg and Jana, for the knowledge and laughter we shared and for taking care of me in such a heartfelt way.

My parents provided for me, incentivized and supported my decisions while also making it possible to study without having to worry about anything else and without having any needs. I feel unworthy of such unconditional and am forever grateful to you. This feeling of gratefulness is extended to my sister, Joana, to whom I wish to thank for taking care of me, whenever I needed. Special thanks to my grandparents, who are still able to inspire and amaze me despite their age.

This project was possible due to the European Community initiative of making students study abroad with the ERASMUS program, to which I am thankful for since it made affordable for me to live in a different country and experience a different culture.

The author wishes to acknowledge the initiative and entities behind this project, that help expand human knowledge. Predicción probabilística de daño y fallo a fatiga: aplicación a componentes y estructuras de materiales poliméricos, Ref. DPI2016-80389-C2-2-R, CONVOCATORIA 2016 DE PROYECTOS DE I+D+I, Ministerio de Economía y Competitividad (Spain).

To Elisa, for her time, patience and perseverance.

Index

Index of figures

Index of tables

Nomenclature

Symbol	Definition
ASTM	American Society for Testing and Materials
COD	Crack opening displacement
CT	Compact tension
EFCDF	Experimental failure cumulative distribution function
GLM	Generalized local model
GP	Generalized parameter
GP_{max}	Maximum generalized parameter
GP_{min}	Minimum generalized parameter
ISO	International Organization for Standardization
PFCDF	Primary failure cumulative distribution function
Std Dev	Standard deviation
WLF	William Landel Ferry
3-PTB	Three-point bending
A	Area
a_T	Temperature shift factor
c	Constant value
cdf	Cumulative distribution function
ΔH	Apparent activation enthalpy
ΔS	Specimen size
e	Prony constant
E	Young's modulus
E_a	Apparent activation enthalpy
F	Force
$\mathcal{H}$	Heaviside step function
J	Creep compliance
K_j	Test number
n	Number of specimens
P_f	Probability of failure
$P_{f,\Delta S}$	Probability of failure for a new size
$P_{f,j}$	Specimen's probability of failure
$P_{s,global}$	Global probability of survival
$P_{s,i}$	Probability of survival per element
R	Boltzmann's constant

R^2	Coefficient of determination
S	Specimen size
S_{eq}	Equivalent size
S_{global}	Global size
S_{ref}	Reference size
t	Time
T	Temperature
T_0	Reference temperature
$W0$	Width overall
x	Failure parameter
$\bar{y}$	Average experimental value
y_i	Experimental value
$\hat{y}_i$	Linear regression value
α	Coefficient of thermal expansion
β	Shape factor
δ	Scale factor
ε	Strain
ε_c	Creep strain
ε_D	Dashpot strain
ε_e	Elastic Strain
ε_0	Initial, constant, strain
ε_P	Plastic strain
ε_S	Spring strain
ε_T	True strain
η	Viscosity
λ	Location parameter
σ	Stress
σ_D	Dashpot stress
σ_{GKV}	Kelvin-Voight generalized model stress
σ_{GM}	Maxwell generalized model stress
σ_0	Initial, constant, stress
σ_S	Spring stress
σ_T	True stress
υ	Poisson’s ratio
τ	Retardation time

ζ	Reduced time

1 Introduction

With the growing demand for components made of or incorporating viscoelastic materials, the full knowledge of the behaviour and durability of using them in different applications is needed. A component that has been built with optimized characteristics will often perform as expected and requires the minimum amount of resources to do so. However, to achieve such feature, it must be designed adequately and that relies deeply on the knowledge of material's mechanical behaviour.

In this project, the fracture behaviour of a commercially available epoxy resin – EPOLAM 2025 – is studied using probabilistic tools. Applying the Generalized Local Model (Calvente 2017), the suitability of the model to characterize viscoelastic materials is going to be assessed as well its transferability among geometries.

EPOLAM 2025 is an epoxy resin commonly used for manufacturing heat-resistant tools, although it is used in wet lay-up, moulding and vacuum bagging processes as well, even for components as large as windmill blades.

Viscoelastic material properties can alter drastically with temperature increments, especially around glass transition temperature. To evaluate EPOLAM 2025 behaviour at ambient temperature, a viscoelastic characterization will be performed through relaxation tests at different temperatures to which the temperature-time transition superposition principle is going to be applied. The resulting master curve for relaxation modulus will be approximated using Prony series.

Tensile tests will also be performed in dogbone specimens and compact tension specimens. Three-parameter Weibull cumulative distribution functions will be fitted to experimental data collected from these experiments, considering the ultimate tensile strength as a generalized parameter and the interchangeability of the generalized local model, applied to this material, will be assessed.

1.1 Context of the project within the IEMES research group

IEMES research group was created with the objective of characterizing materials mechanically and developing probabilistic models to predict the lifetime of structures and structural components under fatigue and fracture.

The group succeed at developing methods of probabilistic characterization (C Przybilla 2014; Muñiz-Calvente et al. 2015) and at characterizing materials, such as glass (Lamela et al. 2014).

There is a gap, however, in characterizing polymeric materials. This thesis is developed as a contribution to fill this gap, applying the previously developed methodologies to an epoxy resin and concluding about the feasibility of such approaches.

1.2 Objectives

The proposed work is developed with the purpose of:

1. Assessing an epoxy resin's viscoelastic behaviour, characterizing its relaxation modulus variation with time. This implies performing transient relaxation tests at different temperatures and applying the Time-Temperature Superposition (TTS) principle to obtain a master curve for the relaxation modulus.
2. Planning, performing and assessing quasi-static tensile and fracture experiments based on the probabilistic models previously developed by IEMES group. This is conducted by
    - Choosing a generalized parameter;
    - Obtaining an experimental failure cumulative distribution function – EFCDF – that allows the primary failure cumulative distribution function – PFCDF – to be obtained by deriving the EFCDF.
    - Assessing the transferability of the PFCDF of the material to another geometry.

1.3 Methodology

This thesis is expected to be developed according to a methodology outlined in the following steps:

1. Perform experimental and numerical analysis of viscoelastic material behaviour. Obtain the material relaxation modulus using the TTS principle and Prony coefficients.
2. Perform an experimental programme of tensile and fracture quasi-static tests of an epoxy resin – EPOLAN 2025.
3. Elaborate a finite element model for the experimental tests, assuming material's behaviour as elastoplastic.
4. Validate the numerical values obtained from the finite element's model, using experimental data.
5. Perform a numerical analysis of the fracture test using the σ–ε experimental curve obtained in the tensile test, under plastic material behaviour.
6. Obtain the PFCDF as a material relative property.

1.4 Structure

This thesis is structured in chapters, according to the following order:

Literature review

This chapter presents a literature review on viscoelastic materials, a review of the generalized local model, size effect and Weibull's probabilistic model theory. An overview of the ordinary least squares (OLS) method is done. Digital image correlation basic principles are described, according to the needs of this project.

Experimental procedure

In this chapter, the tests that will be performed along the project are described. The standards that served as guidelines to the experiments are mentioned, as well as the machinery used. Then, a guide on how the experiments will be performed is presented, taking into account possible assumptions made, software and hardware interactions and respective parameters attributed to each type of test.

Results and discussion

In this chapter, the obtained results are analysed. Possible causes of discrepancies are explored and all considerations exposed.

Conclusions

Comments on the final results and conclusions drawn from the investigation undertaken, as well as a presentation of possible future work to be developed on the subject are presented.

2 Literature review

2.1 Viscoelastic characterization

2.1.1 Viscoelastic behaviour

For the majority of cases, material's behaviour in solid state may be described by Hooke's law of linearity, when subjected to small increments of strain. Hooke's law describes a linear and proportional relationship between the stress σ and the strain ε, as shown in equation 2.1, with E representing Young's modulus.

$$\sigma = \varepsilon \cdot E \tag{2.1}$$

Equation 2.1 can also be written in terms of a compliance J, as shown in equation 2.2, being J the inverse of the Young's modulus, equation 2.3.

$$\varepsilon = J \cdot \sigma \tag{2.2}$$

$$J = \frac{1}{E} \tag{2.3}$$

This behaviour is commonly represented by a purely elastic spring, a mechanical component with a stiffness of E (Figure 1).

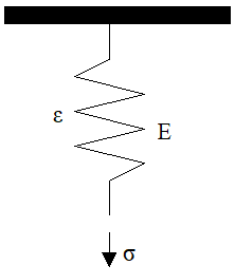

Figure 1 – Spring

If a material is in liquid state, its behaviour under shear stress can be described by Newton's law – equation 2.4 – where shear stress is proportional to the rate of strain $\frac{d\varepsilon}{dt}$ and related to the material's viscosity η.

$$\sigma = \eta \cdot \frac{d\varepsilon}{dt} \tag{2.4}$$

A mechanical component that represents this behaviour is a purely viscous dashpot (Figure 2) in which η represents the dashpot's viscosity coefficient.

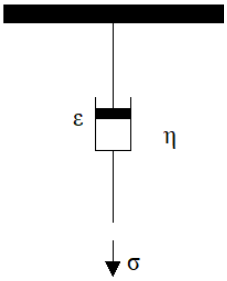

Figure 2 – Dashpot

The classical theory of elasticity uses Hooke's law to relate stress and strain for solids with elastic properties, not taking into account the rate of strain. On the other hand, the classical theory of hydrodynamics relates the stress to the rate of strain through Newton's law, disregarding the strain itself. These concepts work as a guideline and an idealisation, representing material behaviour for infinitesimal variations of strain in solids, and infinitesimal changes in the rate of strain in liquids. Considering infinitesimal variations to be the amount up to which the material behaves as described by these laws, two types of deviations can be considered.

Firstly, whenever a higher than infinitesimal strain is applied to a solid, it suffers non-Hookean deformation – plasticity – and the stress-strain relations are more complex. In a similar way, many fluids in steady flow deviate from Newton's law whenever a higher rate of strain is observed.

Secondly, some materials will share both solid and liquid characteristics. This implies that, whenever a constant stress is applied to a materia, it will not respond with a constant deformation but will, instead, deform increasingly with time. Alternatively, if a constant deformation is applied, it will gradually require a smaller stress to keep the same value. Similarly to liquids, if the material is flowing under a constant stress, it retains some of the energy, instead of dissipating all of it; it recovers part of its original shape as the applied stress is removed. The materials that fall under these two last considerations are known as *viscoelastic* materials.

Given previous considerations – equations 2.1 and 2.4 – it is possible to define a first approach to the equation ruling the behaviour of a viscoelastic material with equation 2.5.

$$\sigma = E \cdot \varepsilon + \eta \cdot \frac{\partial \varepsilon}{\partial t} \tag{2.5}$$

Considering the case in which a constant stress is applied to a viscoelastic material, a continuous deformation will be experienced with its velocity depending on the material's temperature. This phenomenon is known as *creep*.

Creep

For those who had the joy of playing with a chewing gum, stretching it until it breaks apart, creep is already an observed phenomenon. Stretching it at a constant stress will imply a high strain velocity at an early stage, with the cross-section diminishing rapidly at first, followed by a stage where the gum keeps stretching but at a constant velocity, narrowing the cross-section in a much lower rate, and eventually the gum breaks in two pieces with a sudden growth of the deformation rate. This behaviour describes the three general stages of creep: a primary stage, with a decreasing rate of strain; a secondary stage, where a nearly constant rate of strain is observed; and a third or tertiary stage, with an increasing rate of strain leading to fracture.

In Figure 3 strain is represented as a function of time $\varepsilon(t)$ during a creep test, with different creep regimes represented according to the different stages, by different time derivatives $\frac{d\varepsilon}{dt}$.

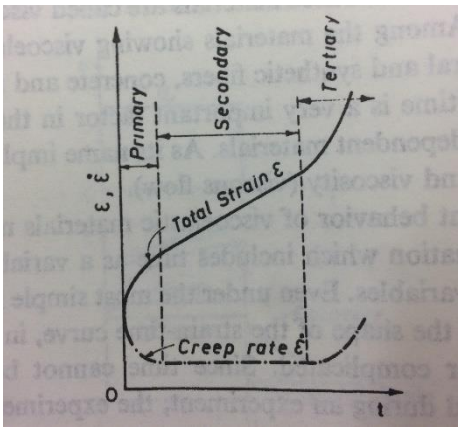

Figure 3 – Three stages of creep (Findley 1978)

Since the material did not lose its ability to recover partially from an applied stress when unloaded, creep strain can be split into two different categories: elastic strain ε_e and creep strain ε_e. The elastic strain is a constant, while creep strain is time dependent, therefore:

$$\varepsilon(t) = \varepsilon_e + \varepsilon_c(t) \tag{2.6}$$

$$\frac{d\varepsilon}{dt} = \frac{d\varepsilon_c}{dt} \tag{2.7}$$

Recovery

The loose skin between the thumb and the index fingers, after pinched, regain its shape. As we age, this feature is not lost but the rate of recovery is often slower because skin loses its elasticity (Ryu et al. 2008). A portion of skin goes back to its original shape at a fast rate, while the rest slowly crawls back to its place. This happens because there is both elastic strain and creep strain, as the elastic strain – like in steel, for instance – recovers its shape almost instantly and the creep strain is time-dependent, recovering at a decreasing velocity – Figure 4.

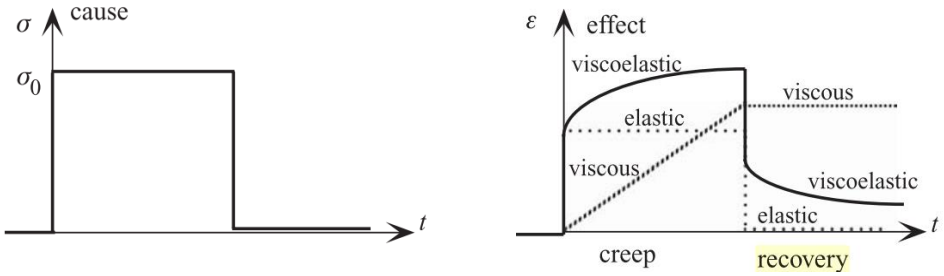

Figure 4 – Creep and recovery for viscoelastic behaviour (Lakes 2009)

It is important to notice that, although the skin between the fingers recovers its full shape as part of the human body, if a viscoelastic material is to be analysed as an isolated system it may not recover the initial shape, independently of the recovery time.

Relaxation

Considering now that, instead of a constant stress, a constant strain is applied to a viscoelastic material, a phenomenon named *relaxation* occurs and the material will require less stress to withstand the same strain.

Humans are pain sensitive and that is one of the reasons why it may be difficult for some to reach their toes while keeping the legs straight. Although, given enough time and practice, it becomes easier and feasible. A good starting point would be to stretch as far as possible and hold the position for a few seconds. It would be painful at first, as the tendons are stressed but,

with time, one would feel less pressured while holding the same position. This happens because tendons relax over time, which helps overcome the pain and venture into stretching more, and leads to improvements as tendons not fully recover the original length (Bonifasi-Lista et al. 2005; Herbert et al. 2002).

Given such behaviour it is possible to conclude that the stress associated with a constant strain is time-dependent and decreasing for viscoelastic materials – Figure 5.

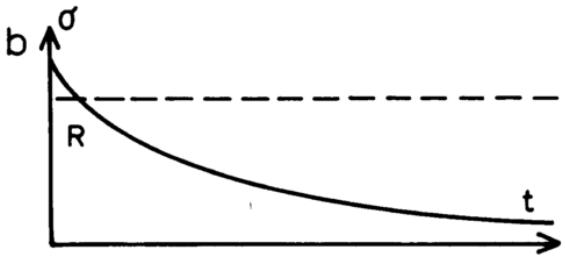

Figure 5 – Relaxation (Kinloch and Young 1984)

Similar to what happens to linear elastic mechanics' applications whenever the plasticity barrier is crossed, the presented considerations are not valid for all viscoelastic materials. Factors ranging from stress, strain, time or temperature will affect the material behaviour and cause it to be linear or nonlinear, this requires a definition of what is a linear viscoelastic material. Nonlinear viscoelastic will be those materials that do not behave as the linear but will not be thoroughly explained as it goes beyond the scope of the present work.

Linear viscoelasticity

For a material to be considered linear it has to be in accordance with two conditions (Findley 1978):

- Stress σ is proportional to strain ε at a given time:

$$\varepsilon[c \cdot \sigma(t)] = c \cdot \varepsilon[\sigma(t)] \tag{2.8}$$

  Taking into consideration that c is a constant, the stress is imposed and strain is a response to that stress; equation 2.8 states that the strain caused by an input of $c\sigma(t)$ must be equal to the strain output times the scalar c, caused by a stress input of $\sigma(t)$.

- A material's behaviour must obey Boltzmann superposition principle (Boltzmann 1876):

  Boltzmann principle states that a compound parameter can be described by the sum of the parameters that form it (Lakes 1998). So, for instance, if a tensile test is applied in a specimen that was in a stress-free state when $t = 0$, the stress $\sigma(t)$ to which it is subjected is a functional of all the strains $\varepsilon(t)$ up to an instant t.

  The same principle can be applied for the strain resulting from the sum of any two different stresses applied at different intervals of time, that is going to be equal to the sum of the resulting strain from applying each of the stress by itself (Figure 6). This can be described by equation 2.9.

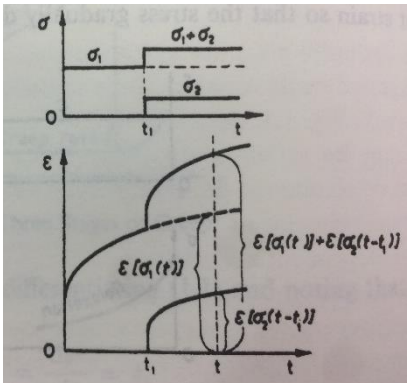

Figure 6 – Boltzmann superposition principle (Findley 1978)

$$\varepsilon[\sigma_1(t) + \sigma_2(t - t_1)] = \varepsilon[\sigma_1(t)] + \varepsilon[\sigma_2(t - t_1)] \tag{2.9}$$

Built on these considerations and considering a Heaviside unit step function – equation 2.10 – the output of a viscoelastic material is a function of not only time t but of the moment the input τ was applied as well.

$$\mathcal{H}(t - \tau) = \begin{cases} 0 & , \quad t < \tau \\ \frac{1}{2} & , \quad t = \tau \\ 1 & , \quad t > \tau \end{cases} \tag{2.10}$$

Being the output a stress, the constitutive equation for a viscoelastic medium is represented in equation 2.11, where $E(t)$ is the *relaxation modulus* of the material. If the output is strain, the constitutive equation is represented by equation 2.12, where $J(t)$ is the *creep compliance* of the material (Lakes 1998).

$$\sigma(t) = \int_0^t E(t - \tau) \cdot \frac{d\varepsilon(\tau)}{d\tau} d\tau \tag{2.11}$$

$$\varepsilon(t) = \int_0^t J(t - \tau) \cdot \frac{d\sigma(\tau)}{d\tau} d\tau \tag{2.12}$$

As shown in Figure 1 and Figure 2, mechanical components are used as references to describe physical behaviours. Combined, as in equation 2.5, they can simulate viscoelastic materials.

One example of such would be a car suspension, where a spring is connected in parallel with a dashpot and the system spring+dashpot is connected to a tire, which acts like a spring (Gündoğdu 2007). The whole system makes the journey easier by acting as viscoelastic, with a lower strain response when a stress is applied – creep – and a smoother recovery once it is unloaded – recovery.

The car suspension system is one of many possible combinations of mechanical components. However, the solution for studying such problems relies on the analysis of the simpler scenarios and then using them as a reference for any other configuration. With that in mind, it is most common to mention the *Maxwell* model – referring to the case where a spring and a dashpot are in series – or to the *Kelvin-Voigt* model – where a spring is connected in parallel with a dashpot.

Mechanical models

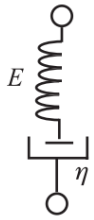

Figure 7 – Mechanical representation of the Maxwell model (Lakes 2009)

The Maxwell model, in which a spring is in series with a dashpot (Figure 7), relies on the principle that under an applied axial force, the stress subjected to the spring σ_S is equal to the stress in the dashpot σ_D and ultimately equal to the total stress σ, while the total deformation ε is equal to the sum of the deformation of the spring ε_S and the deformation of the dashpot ε_D. These considerations take into account the assumption that the deformation is quasi-static, while inertia is neglected, and they can be mathematically defined as follows:

$$\sigma = \sigma_S = \sigma_D \tag{2.13}$$

$$\varepsilon = \varepsilon_S + \varepsilon_D \tag{2.14}$$

Deriving equation 2.14 in time, one obtains

$$\frac{d\varepsilon}{dt} = \frac{d\varepsilon_S}{dt} + \frac{d\varepsilon_D}{dt} \tag{2.15}$$

Which can be further developed by making use of equations 2.1 and 2.4 into

$$\frac{d\varepsilon}{dt} = \frac{d}{dt}\left(\frac{\sigma}{E}\right) + \frac{\sigma}{\eta} \tag{2.16}$$

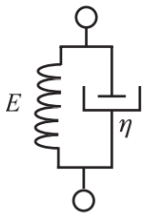

Figure 8 – Mechanical representation of the Kelvin-Voight model (Lakes 2009)

Given the fact that the spring stiffness *E* is constant in time, equation 2.16 can be rearranged as shown in equation 2.17, defining the differential equation of the Maxwell model.

$$\frac{d\varepsilon}{dt} \cdot E = \frac{d\sigma}{dt} + \frac{E}{\eta}\sigma \tag{2.17}$$

The Kelvin-Voigt model, usually referred to as either Kelvin or Voigt model, consists of a spring and a dashpot connected in parallel (Figure 8). Considering one end of the model to be static and assuming an axial force is applied in the opposite end, the resulting stress subjected to the model σ will be the sum of the stress in the spring σ_S and the stress in the dashpot σ_D. The strain of the model ε would be equally suffered by the spring ε_S and by the dashpot ε_D. These relations can be represented as:

$$\sigma = \sigma_S + \sigma_D \tag{2.18}$$

$$\varepsilon = \varepsilon_S = \varepsilon_D \tag{2.19}$$

By substituting equations 2.1 and 2.4 into 2.18, equation 2.20 is deduced and it represents the differential equation that rules the Kelvin-Voigt model.

$$\sigma = E \cdot \varepsilon + \eta \cdot \frac{d\varepsilon}{dt} \tag{2.20}$$

Both the Maxwell and Kelvin-Voight models have a generalized form, used to obtain better approaches and adjustments whenever an experimental result needs to be matched in higher detail. These are obtained by superposition of as many Maxwell models as required or by superposition of Kelvin-Voigt models (Figure 9).

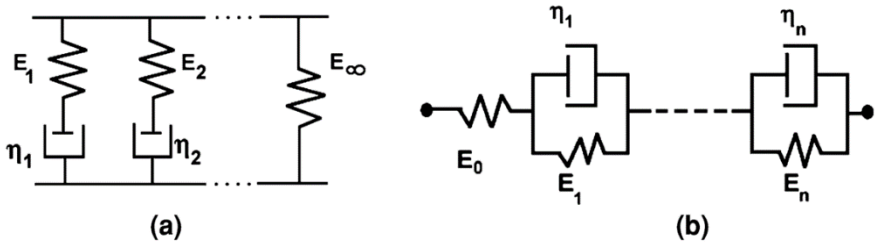

Figure 9 – (a) Maxwell generalized model; (b) Kelvin generalized model (Bott 2014)

- Maxwell generalized model

In Maxwell's generalized model, the stress to which the whole model is subjected σ_{GM} is equal to the sum of all the stresses applied in each of the models' *n* branches.

$$\sigma_{GM} = \sum_{i}^{n} \sigma_i \tag{2.21}$$

- Kelvin-Voigt generalized model

For the Kelvin-Voigt generalized model, the resulting strain ε_{GKV} is the sum of each of the components' strain that is in series.

$$\varepsilon_{GKV} = \sum_{i}^{n} \varepsilon_i \tag{2.22}$$

To assess the properties of viscoelastic materials, experimental methods must be applied. Ferry (1980) separated viscoelastic materials into three categories and defined different types of methodologies for each: viscoelastic liquids; soft viscoelastic solids and liquid with high viscosity; and hard viscoelastic solids. However, generalized tests can be performed in order to establish stress-strain relations and characterize a viscoelastic material by its creep compliance and relaxation modulus.

2.1.2 Experimental assessment

Creep test

The creep compliance $J(t)$ relates the strain output $\varepsilon(t)$ with a steady and fix stress σ_0 that is imposed to a specimen – equation 2.23 (Findley 1978).

$$J(t) = \frac{\varepsilon(t)}{\sigma_0} \tag{2.23}$$

To establish this relation, a static transient test is performed in which a steady force is applied and the strain output recorded. The strain is expected to have a threshold value when the force is applied and then increase in time.

Stress relaxation test

The relaxation modulus $E(t)$ is obtained by relating a steady fix strain ε_0 that is applied to the material, with the variation of stress $\sigma(t)$ – equation 2.24 (Findley 1978).

$$E(t) = \frac{\sigma(t)}{\varepsilon_0} \tag{2.24}$$

This relation is attained from a static transient test and the output stress is expected to reach its peak when the strain is applied and then decrease with time.

The creep compliance relates to the relaxation modulus according to equation 2.25 and 2.26 with equations 2.27, 2.28 and 2.29 being also valid, as described by Findley (1978) and Ferry (1980).

$$\int_0^t J(t-\tau) \cdot E(\tau)\, d\tau = t \tag{2.25}$$

$$\int_0^t E(t-\tau) \cdot J(\tau)\, d\tau = t \tag{2.26}$$

$$E(t) \cdot J(t) \leq 1 \tag{2.27}$$

$$E(0) \cdot J(0) = 1 \tag{2.28}$$

$$E(\infty) \cdot J(\infty) = 1 \tag{2.29}$$

Equations 2.28 and 2.29 are of particular importance as they describe constant values for initial and final moments in a material's behaviour (considering final to be a long time value). These do not depend on time and define glassy and rubbery states, respectively.

It was previously mentioned that viscoelastic behaviour does not only depend on time, it is also temperature related. The relation between the material's parameters and the temperature is of major importance for accurately projecting a component.

Time-temperature superposition principle

Supposing that relaxation moduli $E(T, t)$ were obtained at several different temperatures and taking T_0 as a reference temperature, it is possible to overlap the curves correspondent to each of the temperatures. A reference temperature tests keeps its original time scale, while other tests are adjusted along the horizontal axis, if plotted in logarithmic scales. This methodology is known as time-temperature superposition principle (Leaderman 1941) and if the superposition is in fact possible, the material is called *thermorheologically simple* (Schwarzl and Staverman 1952).

The time t that is originally associated with each of the adjusted temperatures is shaped into a *reduced time* ζ that relates to t through a *temperature shift factor* a_T – equation 2.30. The temperature shift factor is related to the temperature T that is being adjusted, the reference temperature T_0 and an *apparent activation enthalpy* ΔH.

$$\zeta = \frac{t}{a_T(T)} \tag{2.30}$$

For glassy states, the Arrhenius equation – equation 2.31 – gives a good approximation of the material's behaviour (Drozdov 1998), while for rubbery states the WLF equation (Williams,

Landel, and Ferry 1955) gives a more appropriate description of the material's response – equation 2.32.

$$\log a_T(T) = \frac{\Delta H}{R}\left(\frac{1}{T} - \frac{1}{T_0}\right) \tag{2.31}$$

$$\log a_T(T) = -\frac{C_1 \cdot (T - T_0)}{C_2 + T - T_0} \tag{2.32}$$

with

$$C_1 = \frac{\Delta H}{R \cdot f(T_0)} \qquad C_2 = \frac{f(T_0)}{\alpha}$$

Where R is the *Boltzmann's constant*, f represents the *free volume fraction* (Doolittle 1951) and α is the material's *coefficient of thermal expansion*.

The curve resulting from the superposition is named *master curve*. It is important to note that the relaxation modulus obtained in the master curve is now dependent on the reference temperature as well as reduced time, $E\big(T_0; \zeta(t,T)\big)$.

The relaxation function represented by the master curve can be modelled accurately using Prony series as shown by Tzikang (2000). Using equations such as equation 2.33 is often easier than solving convolution integrals such as those represented in equations 2.25 and 2.26, in order to obtain other viscoelastic properties (Fernández 2011). In equation 2.33 e_i is a Prony constant and τ_i represent the Prony retardation time constant ($i = 1,2,\dots,m$).

$$E(t) = E_0\left[1 - \sum_{i=1}^{m} e_i \cdot \left(1 - exp\left(-\frac{t}{\tau_i}\right)\right)\right] \tag{2.33}$$

2.2 Probabilistic characterization of failure

Material's specimens with a given geometry tend to fail around a certain value in similar loading conditions, with more or less deviation depending both on dimensional similarity and construction quality. Ideally, equal specimens would fail under the exact same conditions.

Given this consideration, probability models can be used to describe the likelihood of a material to fail, defining a range of values where it may occur and the probability of happening. When compared with traditional methods, like deterministic models based on finite element analysis, probabilistic models can be more reasonable as they consider scatter from experiments and associate it with a failure probability. In other words, when projecting a component it is useful to define a confidence interval associated with its failure and, therefore, adjust the safety aiming at minimizing material waste and production costs.

A positive point of this type of probabilistic analysis is their general character, allowing their application to any type of parameter, such as fatigue, ultimate monotonic strength, creep or corrosion stress, as well as their suitability of being applied to different types of materials, including glass (Lamela-Rey et al. 2007), steel (Correia, De Jesus, and Fernández-Canteli 2013; Blasón et al. 2017; De Jesus et al. 2010) or polymers (Salazar, Frontini, and Rodríguez 2014; Cocco, Frontini, and Perez Ipiña 2007).

The chosen parameter will show scatter, most of the times related to either a maximum or a minimum value distribution, such events falling under the extreme value theory (Castillo 1988).

2.2.1 Extreme value theory

As extreme values are considered, a limit condition mentioned by Castillo et al. (1985) has to be considered and it implies the use of stable asymptotic families of probability distributions, which are Weibull, Fréchet and Gumbel. Each of these families can express a maximum or a minimum value and are often used to model unusual events such as natural disasters.

A starting point to assess a material's failure condition is considering that it does not fail until a threshold value of the selected parameter. Knowing so, Fréchet's distribution function for minima can be disregarded as its lower tail continues up to minus infinity. Also, it is fair to assume that above a certain value the material will inevitably fail – as it would happen if crack propagation was the considered parameter. As Fréchet's distribution function for maxima presents a limitless upper tail, it will also be disregarded. As mentioned by Calvente (2017), and considering only minima distribution functions, when the shape factor reaches relatively high values, Gumbel's distribution function can be taken as a limiting case of Weibull's distribution function for minima. As such, a three-parameter Weibull cumulative distribution function (cdf) for minima is considered – Figure 10.

2.2.2 The Weibull distribution function

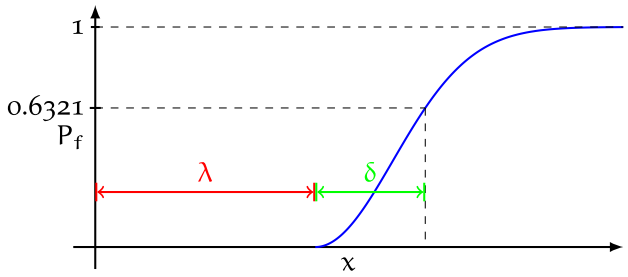

Figure 10 – Weibull cumulative distribution function for *minima* (Przybilla 2014)

Presented by Weibull (1939) and labelled as a statistical distribution function of wide applicability (Weibull 1951), Weibull's distribution function – equation 2.34 – represents an accumulated probability P_f as a function of a failure parameter x, which is related to three Weibull parameters: a *location parameter* λ; a *shape factor* β; and a *scale factor* δ.

$$P_f(x) = 1 - exp\left[-\left(\frac{x-\lambda}{\delta}\right)^{\beta}\right] \tag{2.34}$$

where

$$x \geq \lambda \quad ; \quad -\infty < \lambda < +\infty \quad ; \quad \delta > 0 \quad ; \quad \beta > 0$$

The location parameter λ represents a minimum threshold, under which failure does not occur, meaning a zero failure probability for the x values which are under λ. Some authors consider this value to be equal to zero (Loidl et al. 2007; Wang and Xia 1998), which does simplify the model but is laid on the conservative principle that close to zero values have a probability of failure. If, for instance, we consider a brand-new chair as an object of study, the user's weight is not expected to break it. Although, given sufficient use, aging, corrosion and any other factor that can affect the materials, the likelihood of failing with its user's weight increases and may reach a point where it collapses on its own, with a close to zero value. However, the application of the Weibull cdf takes in consideration a single failure parameter and that could be any of the mentioned in the chair example. For such reason, λ is considered is this work.

The shape factor β is inversely proportional to the data scatter and relates to the distribution's slope; this means that higher scatter are associated with low shape factors and vice-versa. This

parameter can be used to assess the material's quality, as a high value will mean lower scatter and a more reliable material, with less flaw density (Weil and Daniel 1964).

The scale factor δ relates to the analysed specimen's geometry, i.e. the specimen size S at failure. This is of particular importance because, as long as there is a uniform distribution of x along any geometry, it can be described by a Weibull cdf and, moreover, related to any other specimen size ΔS through a new scale factor δ_{new} – equation 2.35 (Calvente 2017).

$$\delta_{new} = \delta \cdot \left(\frac{S}{\Delta S}\right)^{1/\beta} \tag{2.35}$$

Substituting equation 2.35 into equation 2.34, it is possible to obtain a relation between a failure parameter of a given geometry with any other size – equation 2.36.

$$P_{f,\Delta S}(x) = 1 - \left[-\frac{\Delta S}{S}\left(\frac{x-\lambda}{\delta}\right)^{\beta}\right] \tag{2.36}$$

As represented in Figure 10, the probability of failure resulting from the sum of the location with the scale factor, equals a constant – equation 2.37. Taking into consideration that the location parameter does not alter when *scale effect* is used (regarding the use of equation 2.36 (C Przybilla 2014)), it is verified that a larger size would present smaller scatter values, close to the location parameter, and a smaller size would account for wider scatter.

$$P_f(\lambda + \delta) = 0.6321 \tag{2.37}$$

Weakest link principle

Presented in Weibull's work (1951), the weakest link principle states that the probability of a mesh survival $P_{s,global}$ is equal to the probability of none of its n elements failing $P_{s,i}$ – equation 2.38. Weibull explains this principle with a chain: assuming that a chain with n links fails whenever one of its links fails, so as long as each of its links remains intact the chain does not fail.

$$P_{s,global} = \prod_{i=1}^{n} P_{s,i} = \left(P_{s,i}\right)^n \tag{2.38}$$

Knowing that the probability of survival is equal to the difference between the overall probability and the failure probability, $P_{s,i}$ can be described by equation 2.39 from equation 2.34. Substituting equation 2.39 into 2.38, a general equation for the global probability of survival is obtained – equation 2.40 – bearing in mind that the global size S_{global} is equal to an element size $S_{element}$ times the number of elements n, i.e. $S_{global} = n \cdot S_{element}$ (C Przybilla 2014).

$$P_{s,i} = 1 - P_{f,i} = exp\left[-\left(\frac{x-\lambda}{\delta}\right)^{\beta}\right] \tag{2.39}$$

$$P_{s,global} = exp\left[-\frac{S_{global}}{S_{element}} \cdot \left(\frac{x-\lambda}{\delta}\right)^{\beta}\right] \tag{2.40}$$

Equation 2.40 gives, in a generalized way, an appropriate mathematical fitting for the size effect on a solid's failure (considering equal sizes among elements).

The size effect

Let's consider the stress definition where stress is equal to a force divided by the area where the force is being applied. This can be represented through a deterministic relation by considering a force F_1 divided by an area A_1 that is equal to a greater (or smaller) force F_2

divided by a greater (or smaller) area A_2 and ultimately equal to a stress σ, as long as the force and the area increase (or decrease) in the same proportion, equation 2.41.

$$\frac{F_1}{A_1} = \frac{F_2}{A_2} = \sigma \tag{2.41}$$

However, the failure probability of a larger specimen is not the same of a smaller specimen, under the same stress condition. This is due to the higher probability of a larger specimen having a defect that could cause it to fail. Going back to Weibull's example, the probability of a chain having a defect that leads to its collapse is higher than the probability of each individual link having a defect that could make it collapse, for the same applied stress. So, whenever a Weibull cdf is obtained to describe a material's behaviour according to experimental tests under uniaxial loading and uniformly distributed stress, it seems unpractical to apply it to another geometry where there are stress variations along the elements without further considerations.

Weil and Daniel (1964) developed a method to calculate Weibull's parameters applicable to 4-point bending structures with both surface and volumetric flaws, where a non-uniform loading occurs, making use of *minimization of least squares* method for a resin.

Beremin et al. (1983) proposed the *local failure model* where an equivalent stress approach is made and a two-parameter Weibull cdf is used. Xia and Shih (1996) considered Beremin's model with a third parameter σ_{th} while characterizing cleavage fracture in steel.

García Prieto (2001) introduced a methodology to obtain what is referred to as *equivalent reference area*, an estimation that takes in consideration both size effect and the weakest link principle for a variable failure parameter along the specimen. These considerations were applied to 4-point bending tests with glass. Przybilla (2011, 2013) built on García's work further developed this concept, applying it to 3-point and 4-point bending specimens and characterizing glass and ceramics. Calvente (2017) took on Przybilla's work and included the probabilistic characterization of ductile materials, creating a model that considers ultimate tensile strength constant all over the elements, in place of the variable stress state, and then derives an *equivalent size* of the specimen – this is referred to as *generalized local model* (Calvente et al. 2015).

2.2.3 Generalized Local Model

The Generalized Local Model aims at defining a *primary failure cumulative distribution function* (PFCDF) as a material property, related to a specific element size – *reference size* – and a *generalized parameter* (GP). Knowing the material's PFCDF enables the probability characterization of failure in any type of elements, considering their shape, size or loading condition. This model is particularly ambitious as it can be used to related finite element method (FEM) results with a failure probability in each of the elements. The PFCDF is derived from an *experimental failure cumulative distribution function* (EFCDF) that is originated by iteratively fitting a three-parametric Weibull distribution to experimental data.

Generalized parameter

The generalized parameter is what has so far been described as a failure parameter. It can represent the critical value associated with failure, whether it is stress, strain, crack length or any other parameter used to design components. The generalized parameter has to be carefully chosen, as it should be a parameter suitable for being reproduced in all types of desired tests.

Equivalent size

Considering a non-uniformly loaded specimen and subjecting its maximum value GP_{max} to another, imaginary, specimen but considering their failure probabilities to be the same, the dimensions of this imaginary specimen would be an equivalent size S_{eq}. It is determined using

equation 2.44. This consideration is to be applied to the full extent of the specimen, disregarding its elements.

Experimental failure cumulative distribution function

Having chosen an adequate generalized parameter, Bernard and Bosi-Levenbach (1953) formula – equation 2.42 – is to be applied to GP in ascending order of magnitude, which assigns a probability of failure to each of the GPs. K_j stands for the test number in the ascending order and n for the total number of tests.

$$P_{f_j} = \frac{K_j - 0.3}{n + 0.4} \tag{2.42}$$

Rewriting equation 2.36 for a user-defined reference size S_{ref} and considering the weakest link principle it is possible to determine the global probability of failure for each test j regarding each element i, with its respective $GP_{i,j}$ – equation 2.43.

$$P_{f,global_i} = 1 - \prod_{i=1}^{n} \left(exp\left[-\frac{S_{eq_j}}{S_{ref}} \left(\frac{GP_{i,j} - \lambda}{\delta} \right)^{\beta} \right] \right) \tag{2.43}$$

In case the element's equivalent size S_{eq_j} is not known a priori (it could be if considering a constant GP along a dogbone specimen's middle section with a known geometry, for instance) it should be estimated by assigning to it a value close to 80% of the specimen original size and the global probability of failure $P_{f,global_i}$ should be taken as equal to the test probability of failure P_{f_j} for a first iteration. Successive iterations should be done by substituting those values in equations 2.43 and 2.44 until it converges, as described by Calvente (2017).

$$S_{eq_j} = -\log\left(1 - P_{f,global_j}\right) \cdot S_{ref} \cdot \left(\frac{\delta}{GP_{max_j} - \lambda} \right)^{\beta} \tag{2.44}$$

Once these values are estimated for all failure results, the Weibull parameters can be approximated by using a linear regression of type $y = Ax + B$, where

$$x = \log\left(GP_{max_i} - \lambda\right) \tag{2.45}$$

$$y = \log\left(-\log\left(1 - P_{f_j}\right) \cdot \frac{S_{ref}}{S_{eq_j}} \right) \tag{2.46}$$

$$A = \beta \tag{2.47}$$

$$B = -\beta \cdot \log(\delta) \tag{2.48}$$

The optimal location parameter λ is reached by maximizing the adjustment of the linear regression using the least square method (Przybilla 2011) and the other parameters by making the required mathematical adjustments to equations 2.47 and 2.48. Replacing the parameters into 2.43 will return the EFCDF. This process is represented through the flowchart in Figure 11.

Primary failure cumulative distribution function

To derive a primary failure cumulative distribution function from the EFCDF, a reference size S_{ref} must be chosen, with unitary values often used for simplification purposes. Then, Weibull's parameters for the PFCDF can be calculated in the same way as presented for the EFCDF. Substituting the parameters into equation 2.49 will return the PFCDF. Bearing in mind that the only changing parameter from the EFCDF must be the shape parameter because, as mentioned before, scatter is size dependant.

$$P_{f_i} = 1 - exp\left[-\frac{S_{eq_j}}{S_{ref}} \cdot \left(\frac{GP_{max_i} - \lambda}{\delta}\right)\right]^{\beta} \tag{2.49}$$

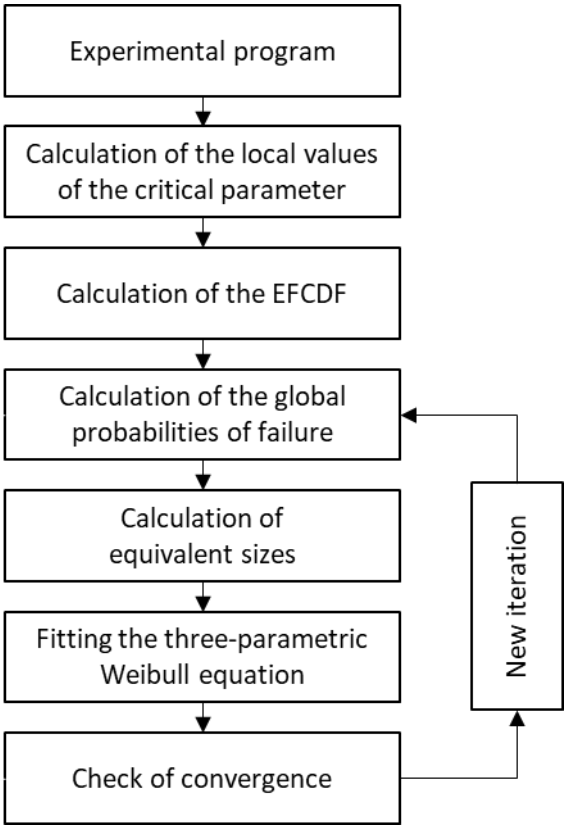

Figure 11 – Flowchart of the Generalized Local Model (Calvente 2017)

2.3 The ordinary least squares method

The ordinary least squares (OLS) method is mentioned throughout this thesis as it is a powerful statistical tool to assess the fit of linear regressions to data.

Let's start by considering random scattered data, as the one plotted in Figure 12, for n points in a coordinate plane. If a line defined by the equation $\hat{y} = m \cdot x + b$ is drawn between those points and the x values are considered as correct, in the sense that they match both the line and the random data, it is possible to determine the variation e_i associated with the vertical distance that goes from the data to the line by simply subtracting the calculated values of $\hat{y}_i$ along the line to the data y_i – equation 2.50.

$$e_i(x_i) = y_i - \hat{y}_i \quad , \quad i = 1 \dots n \tag{2.50}$$

In order to assess the variation of all points, a sum of the variations corresponding to each data point is done. However, using equation 2.50, it would return both positive and negative values, depending on the data, that would nullify each other and give a distorted view of the total error. To avoid this issue, the squared error is calculated instead, as the square parabola presents a unique minimum value and it is easier to operate than higher exponents. As such, the squared variation e^2 would appear as the sum of the squared variations – equation 2.51.

$$e^2 = \sum_{i=1}^{n} (y_i - \hat{y}_i)^2 \tag{2.51}$$

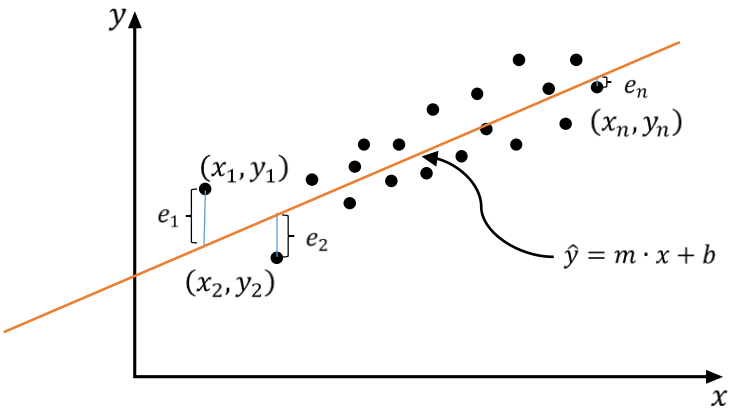

Figure 12 – Random scattered data, fitted through a regression line of type $y = mx + b$

Knowing that $\hat{y}_i = m \cdot x_i + b$ and $i = 1 \dots n$, is it possible to develop equation 2.51 in terms of e^2, m and b – equation 2.52 – and consequently, it is possible to partially derive the resulting equation to obtain a minimum value of both m and b by making the partial derivative equal to zero in both cases – equation 2.53 and 2.54.

$$e^2 = n \cdot \overline{y^2} - 2mn \cdot \overline{xy} - 2bn \cdot \bar{y} + m^2 n \cdot \overline{x^2} + 2mbn \cdot \bar{x} + nb^2 \tag{2.52}$$

$$\frac{\partial(e^2)}{\partial m} = -2n \cdot \overline{xy} + 2mn \cdot \overline{x^2} + 2bn \cdot \bar{x} = 0 \tag{2.53}$$

$$\frac{\partial(e^2)}{\partial b} = -2n \cdot \bar{y} + 2mn \cdot \bar{x} + 2bn = 0 \tag{2.54}$$

Performing algebraic manipulations, it is possible to reach equations 2.55 and 2.56 from equations 2.53 and 2.54, respectively. Equation 2.55 can be further develop into equation 2.57 and then equation 2.57 substituted into 2.56, originating equation 2.58, to represent an optimal slope m and horizontal axis intersection b and equation 2.56 implies that the average value of the data lies on the line that best fits the data.

$$\overline{xy} = m \cdot \overline{x^2} + b \cdot \bar{x} \tag{2.55}$$

$$\bar{y} = m \cdot \bar{x} + b \tag{2.56}$$

$$m = \frac{\bar{x} \cdot \bar{y} - \overline{xy}}{(\bar{x})^2 - \overline{x^2}} \tag{2.57}$$

$$b = \bar{y} - \frac{\bar{x} \cdot \bar{y} - \overline{xy}}{(\bar{x})^2 - \overline{x^2}} \cdot \bar{x} \tag{2.58}$$

Now, assuming the line $\hat{y} = m \cdot x + b$ is drawn to fit the random scattered data previously mentioned, to assess how much this line deviates from what would be an optimal line, the coefficient of determination R^2 is used. The coefficient of determination represents the amount of total variation in y that is described by the variation along x, being the total variation calculated between the data points and their arithmetic mean – equation 2.59. Dividing the variation along the line by the total variation, the amount of variation that is not described by the linear regression is determined. To calculate the amount of variation that is described, one simply has to subtract the obtained value from the unitary value – equation 2.60.

$$Total\ variation = \sum_{i=1}^{n} (y_i - \bar{y})^2 \tag{2.59}$$

$$R^2 = 1 - \frac{\sum_{i=1}^{n}(y_i - \hat{y}_i)^2}{\sum_{i=1}^{n}(y_i - \bar{y})^2} \tag{2.60}$$

2.4 Digital image correlation

Digital image correlation (DIC) is a non-contact measurement methodology that relies on high-resolution cameras to measure displacements in an object surface. Its basic principle relies in correlating the pixels of two digital images of the same object, taken at different instants. For the comparison, an image of the object is selected and assigned as the *reference* image – usually the image taken at the beginning of an experiment – and all the other images are named as *deformed* images – taken throughout the experiment – and making it possible to analyse the displacement field at established time intervals.

The image correlation is done by finding equivalent pixels in both the reference image and the deformed image taken after. To facilitate this task, a pattern is assigned to the surface (made out of dots, lines, grids or random arrays) and the pattern variations arranged into sub regions.

The pixels' correlation relies on two main assumptions. Firstly, the displacement registered between two pixels of the image pattern is assumed to correspond directly to the displacement suffered between two equivalent points on the object. Secondly, the considered sub regions are assumed to have an amount of contrast between them that allows an accurate mapping of their pixels' displacement.

A pinhole camera model is used and the pinhole taken as the referential for the coordinate system – Figure 13. This allows a mapping of the pixels, attributing them coordinates whenever a correlation is performed. If the displacement between two pixels is not null, it can be related to the displacement that occurred on the object's surface, by relating the image resolution with the actual length of the object. To ensure a correct measurement, the image plane must be parallel to the object plane (Sutton 2008).

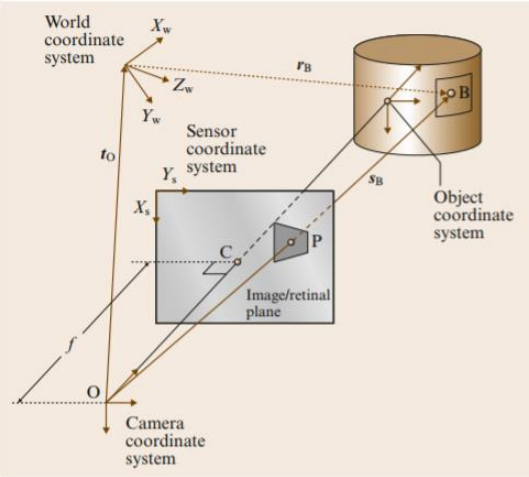

Figure 13 – Scheme of the coordinate system, considering a pinhole camera model (Sutton 2008)

To obtain a random pattern, ensuring a good contrast, it is common to coat the surface with white spray ink and then spray black ink, ensuring patterns up to $50\mu m$ (Sutton 2008). Other processes used rely on applying the same layer of white spray ink but then covering the surface with black toner powder, a patterned vinyl sheet or manually imprinting a pattern with an indelible marker, for instance, or simply polishing, etching or degreasing the object surface. These patterns create unique surroundings for the pixels that are being correlated, making them easier to track precisely based on the pixels that are located around them, as the probability of two pixels in the same image having the same surroundings is lower than comparing pixels based on their brightness (Pan et al. 2009).

The displacements of a planar surface can be obtained through a two-dimensional (2-D) DIC for planar surfaces using one camera only (Sutton 2008) as long as the surface stays planar and, therefore, parallel to the retina plane. When a planar surface deforms its position relative to the sensor plane could change significantly from perpendicularity, requiring an additional camera to take in account the alterations suffered in the direction orthogonal to the surface plane – three-dimensional (3-D) DIC. This 3-D DIC can also be used for analysis of initial curved surfaces.

3 Experimental procedure

All the specimens that were used in the experiments performed along this chapter were supplied by the same companies. The resin and hardener were supplied by AXSON Technologies Spain (Barcelona, Spain), the mixing and curing process was carried by the Instituto Nacional de Técnica Aeroespacial (Madrid, Spain) and the machining of the specimens was performed by Prodintec (Gijón, Spain).

The material is sold under the commercial name EPOLAM 2025 (APPENDIX A) and usually delivered for machining in sheets of material with the desired thickness. These sheets are obtained by pouring the mixture of resin+hardener into a container, where it settles for a fixed amount of time – curing. The curing method leaves a texture on the specimens' surface that is smooth on the surface that is in contact with the container where it is poured. However, the opposite surface is slightly rougher and has a coarse texture. They were named as smooth and free surface, respectively. Three types of specimens were cut from the plates, which are described in the following points:

- 3-point bending specimens

Beam-shaped specimens are used with 50 x 12 x 3mm dimensions, the geometry is based on specimens recommended by ASTM D5023 (2001) – Figure 14. These specimens are cut from a sheet with the same thickness as the beam, all from the same sheet, and then numbered in sequence as they are used for tests, on the free surface.

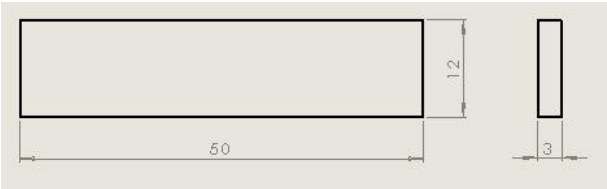

Figure 14 – Geometry and dimensions of the three-point bending specimens

- Dogbone specimens

The dogbone specimens have a type IV geometry as described by ASTM D638 (2004) with a overall width WO of 22mm, within the stipulated tolerance – Figure 15. These were cut out of three different sheets of resin with the thickness of the specimens, marked per sheet (EXX, being XX the sheet number and E standing for EPOLAM) and then numbered twice – one in each end on the specimen – without any specific order or side.

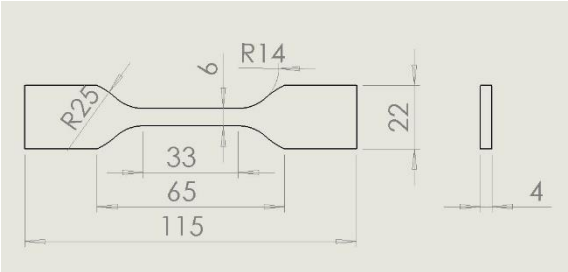

Figure 15 – Geometry and dimensions of the dogbone specimens

- CT specimens

The compact tension (CT) specimens have a geometry based on ISO 13586:2000, with the width w equal to 40 mm, a thickness B of 10 mm and a notched tip, with a 0.24 mm radius. These specimens are cut from a sheet with same thickness of the specimen, all from the same sheet, and numbered in the three edges that do not contain the crack, in sequence as they are used – Figure 16.

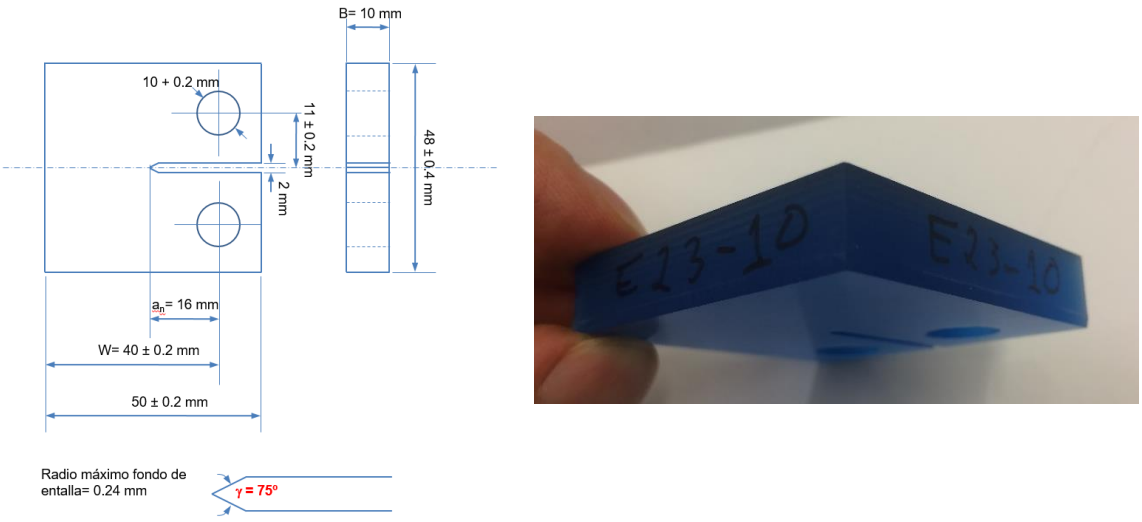

Figure 16 – CT specimen geometry, dimensions and adopted numbering system

All the specimens are stored in airtight containers at ambient temperature, only removed for either testing or analysis.

3.1 Viscoelastic test

To assess the material's viscoelastic properties, relaxation tests are performed. A 3-point bending analysis (3-PTB) is chosen and a rheometric scientific analyser – RSA-III – (Figure 17) was used to perform the tests.

Figure 17 – Rheometric Scientific Analyser – RSA-III

The RSA-III consists of four main pieces of hardware: an oven, used to control the temperature in an insulated chamber with either nitrogen or air; a servo linear actuator with a 3-PTB apparatus installed (Figure 18), used to impose a strain on the material; a thermally insulated chamber, with a thermocouple to measure of the temperature and two resistances that heat the flow of gas originated in the oven; a computer, that runs the software – *TA Orchestrator* – capable of tracking the force values applied by the actuator and the temperature inside the sealed camera.

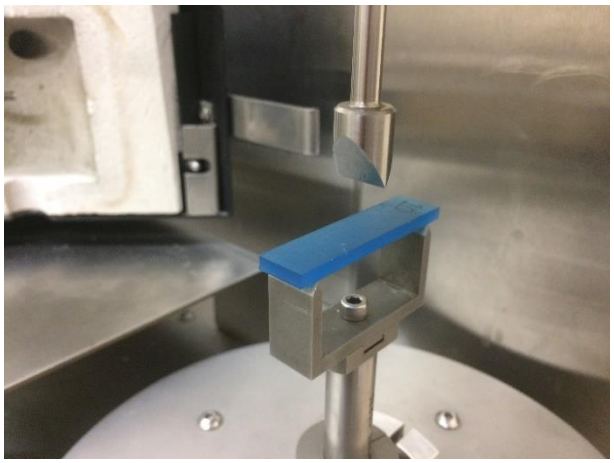

Figure 18 – Three-point bending test

TA Orchestrator allows the user to interact directly with the machine's parameters, being able to define oven's temperature, type of test and offsets. To ensure a minimal error, a force offset was performed after placing the three-point bending apparatus and in-between each test.

Air was used to either cool or heat the sample, provided by a compressor located in a machine's house outside the laboratory. There was no measure of its composition, purity or rate of flow.

The 3-PTB support span has a length of $40mm$, which gives a span-to-depth ratio of 13.3(3) – equation 3.1.

$$\frac{span}{depth} = \frac{40}{3} \cong 13.3(3) \tag{3.1}$$

A 0.1% strain is used as a maximum parameter for steady transient compression, a contacting force of around 0.05N (5g) is applied (this increases for around 0.07N (7g) whenever the oven chamber is used) and two fundamentally different types of tests are performed:

- Ambient temperature test

A first analysis is made without the use of the oven, in short periods of time, with a zone time of four intervals as 1-10-50-100, for a total of 161 seconds while collecting data at a rate of 50 points per zone time.

This test is used to have a glance at the material relaxation modulus and is performed by applying a load through a load indenter that is in contact with the free surface and in another test with the smooth surface (the surface that was in contact with the mould). The tests are performed in both surfaces to assess the beam curvature of the specimen. Each test is repeated three times on each surface, spaced by a 5-minute break to allow the material to regain its shape (relaxation).

- Fixed temperature test

For these experiments, the oven is turned on and the chamber used, a temperature is set as desired and the specimen is allowed to either cool or warm for around ten minutes, to avoid a temperature gradient. The contacting force is then applied and a zone time of 1-10-100-1000 is set, for a total time of 1111 seconds, while collecting 100 points per zone. The tests are performed from 20°C up to 100°C using increments of 10°C.

The same software allows the user to shift the data collected for each temperature into a *TTS Overlay Curve*. This implies the selection of a reference temperature – which is considered 60°C in this work, for no other reason than being an average temperature of the testing range. A high accuracy/slow convergence was chosen with cubic spline interpolation and residual minimization, while the shift method was limited to horizontal only – these parameters defined the TTS defaults (Press et al. 1987). The best fit of the a_T values to Arrhenius' curve is performed, taking in consideration the least squares method.

When a satisfactory fit is obtained, a data reduction can be done as well as a window smoothing, to minimize residues, resulting in the master curve.

The master curve is approximated by a Prony series with thirteen terms, through a *MATLAB*® function. Thirteen terms are used as it is the maximum number of values that can be used to define a viscoelastic material using FEM analysis's software *ABAQUS*™.

3.2 Tensile test

Tensile tests with dogbone specimens were performed according to ASTM D638 (2004).

Type IV specimens are used in a range of temperatures that fluctuate from 14 to 17°C, in a total of twenty-five specimens. The specimens are to be tested at 5 mm/min and the displacement measured with an *MTS 634.31F-24* extensometer – of initial distance L_0 equal to 20 mm, mounted directly to the specimen – Figure 19. The values corresponding to ultimate tensile strength, elongation at break and modulus of elasticity were computed.

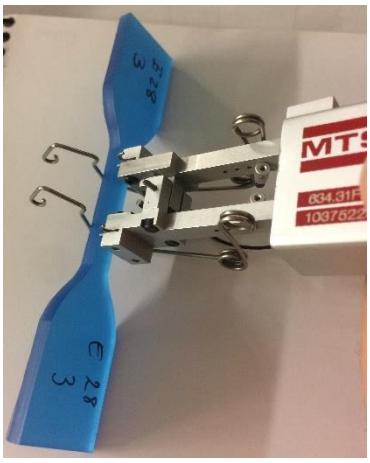

Figure 19 – Extensometer mounted on a dogbone specimen

The Poisson's ratio of the material is obtained using ARAMIS 5M 3-D from GOM – Figure 20. The transversal and longitudinal displacements were obtained according to the specifications shown in APPENDIX B.

Figure 20 – ARAMIS 5M setup

The surface of the material is coated with white spray ink and then sprayed with black ink – Figure 21 – and then a digital photograph is taken at the instant the test starts (reference image), followed by a succession of photographs (deformed images) taken at a frequency of $1Hz$.

Figure 21 – ARAMIS specimen with random, sprayed, pattern

By using ARAMIS software, the DIC method allows the comparison of the sub regions of the initial image with the equivalent sub regions of the following images and is able to keep track of displacement that occur on pixels of these sub regions by analysing the patterns created by the colour contrast. Knowing the resulting displacement, one can easily calculate the deformation allocated to these points, ε, by dividing the displacement between the points Δl by their original distance l – equation 3.2.

$$\varepsilon = \frac{\Delta l}{l} \tag{3.2}$$

Poisson's ratio ν describes the ratio of transversal strain ε_T by longitudinal strain ε_L along a surface – equation 3.3 – and can be assessed by this method, as any other strain in any desired orientation.

$$\nu = \frac{\varepsilon_T}{\varepsilon_L} \tag{3.3}$$

A numerical simulation was performed in *ABAQUS*™ (*version 6.12*,) to assess the validity of fitting a numerical model to the experimental data. The experimental values of specimen E28-2 are going to be used, as it has a higher value for the ultimate tensile strength. The engineering stress σ, recorded directly throughout the test, is converted to true stress σ_T with equation 3.2. True strain ε_T is calculated upon equation 3.3 and then plastic strain ε_P by equation 3.4. The material is assumed to behave as linear elastic behaviour up to the last negative or first zero value of plastic strain and then it enters into plasticity, the plasticity parameters (stress-strain data points) are presented in APPENDIX D. A model is created and meshed appropriately and a numerical simulation performed.

$$\sigma_T = \sigma \times (1 + \varepsilon) \tag{3.2}$$

$$\varepsilon_T = \ln(1 + \varepsilon) \tag{3.3}$$

$$\varepsilon_P = \varepsilon_T - \frac{\sigma_T}{E} \tag{3.4}$$

Applying equation 2.42 to the experimental data and considering the ultimate tensile strength to be the generalized parameter, it is possible to obtain a probability of failure associated with each experimental test. Performing the linear regression presented in section 2.2.2, the Weibull's parameters can be obtained and the EFCDF associated with them. Then, a PFCDF for a reference size of 1mm^3 is derived from the EFCDF.

3.3 Compact test

To validate the GLM model, another geometry is tested and the global probability of failure derived from the PFCDF parameters, applied to the reference size of the new geometry and compared to the experimental data.

Three notched specimens are loaded axially under similar conditions of those presented in section 3.2, with displacement rate of $5mm/min$. The outcome of these tests are force and time.

A numerical model was generated for this specimen in *ABAQUS*™, to calculate the ultimate tensile strength they are subjected to whenever the max load recorded in the experimental test is applied, to characterize the material the same data from the dogbone specimen was used – Young modulus, Poisson's ratio and plastic behaviour characterization. The model is meshed, the resulting input file is loaded into *Abaqus2matlab* (Papazafeiropoulos et al. 2017) and the element volumes and stresses in the main directions imported to *MATLAB*® through *Abaqus2matlab*.

When in *MATLAB*®, a constant distribution of the generalized parameter is assumed in each of the mesh's elements and the global probability of failure of the specimen is calculated using equation 2.43 and plotted versus the experimental data points.

4 Results and discussion

4.1 Viscoelastic results

Six initial tests were performed in RSA-III, analysing both surfaces of three specimens. The test consisted in applying a steady deformation that requires a smaller stress to be applied in time as the material relaxes – Figure 22 and Figure 23.

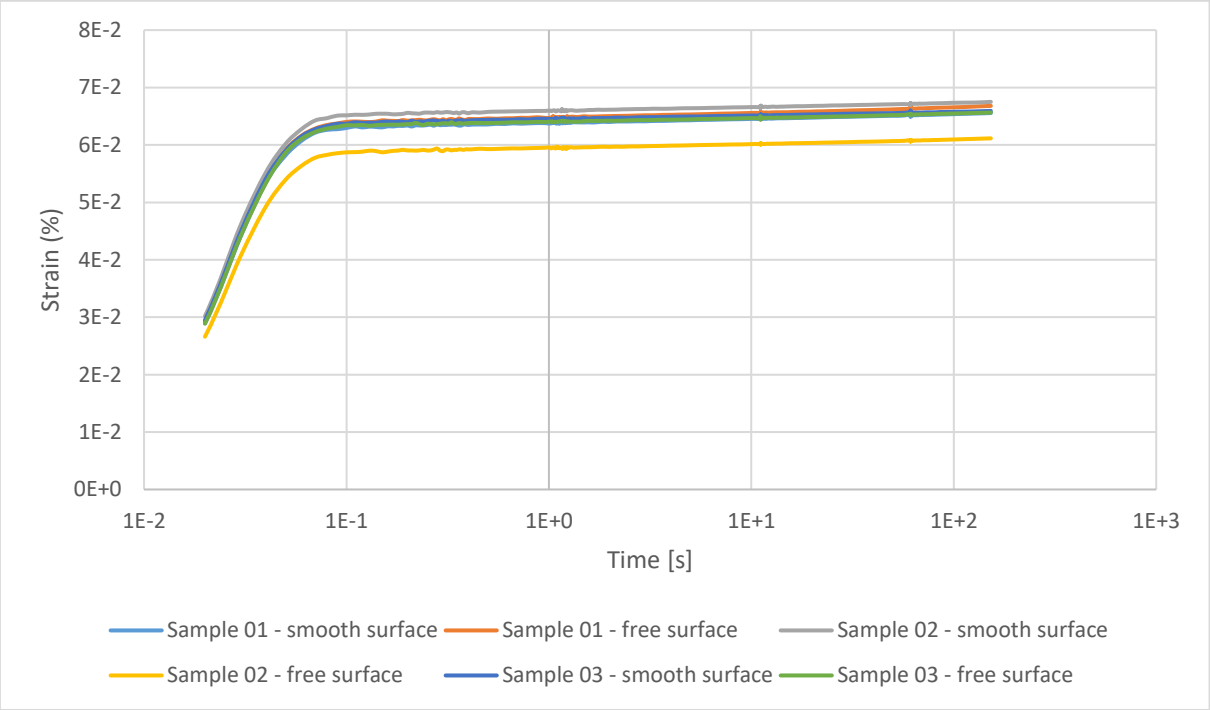

Figure 22 – Steady strain imposed in ambient temperature viscoelastic relaxation tests

The samples were tested alternately, so that they can regain their original shape between tests. A notorious difference of strain is observed in the free surface of sample 02, such a deviance is replicated in the amount of force needed to cause that strain. If a higher force is required to cause a smaller strain, the relaxation modulus is expected to present a higher value.

The values obtained for the relaxation modulus are presented in Figure 24.

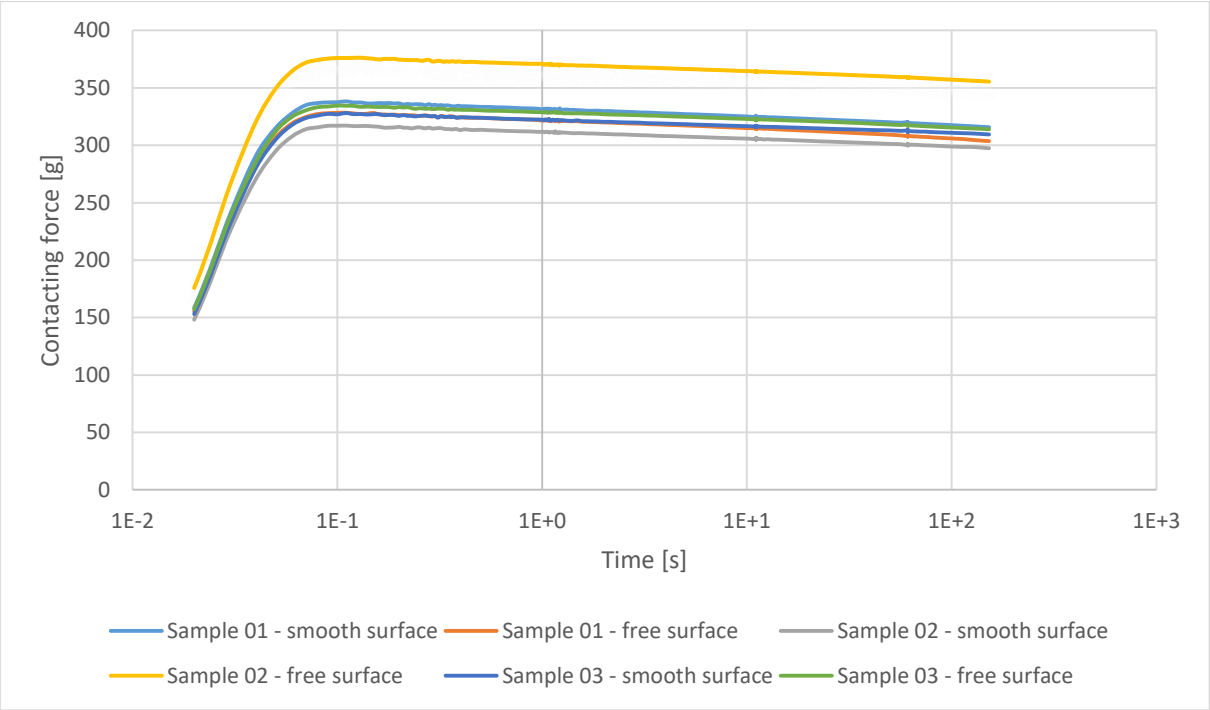

Figure 23 – Input values of force for ambient temperature viscoelastic relaxation test

Sample 02 presents a relaxation modulus in the free surface that is significantly higher than samples 01 or 03 – 2.95 GPa from sample 02 compared to 2.43 GPa of sample 01 and 2.42 GPa of sample 03 – and notoriously lower in the smooth surface – 2.19 GPa as opposed to 2.43 GPa of sample 01 and 2.31 GPa of sample 03 - Figure 24. This phenomenon can be explained by a slight curvature in the beam and accounts for their variation between surfaces but affects sample 02 more than the others. The cause of such curvature can be originated while the resin is settling, after the pouring process, due to a gradient of temperature along the sheet that may lead to residual stresses and, in that sense, the location from where the beams are cut from seems to affect the final result.

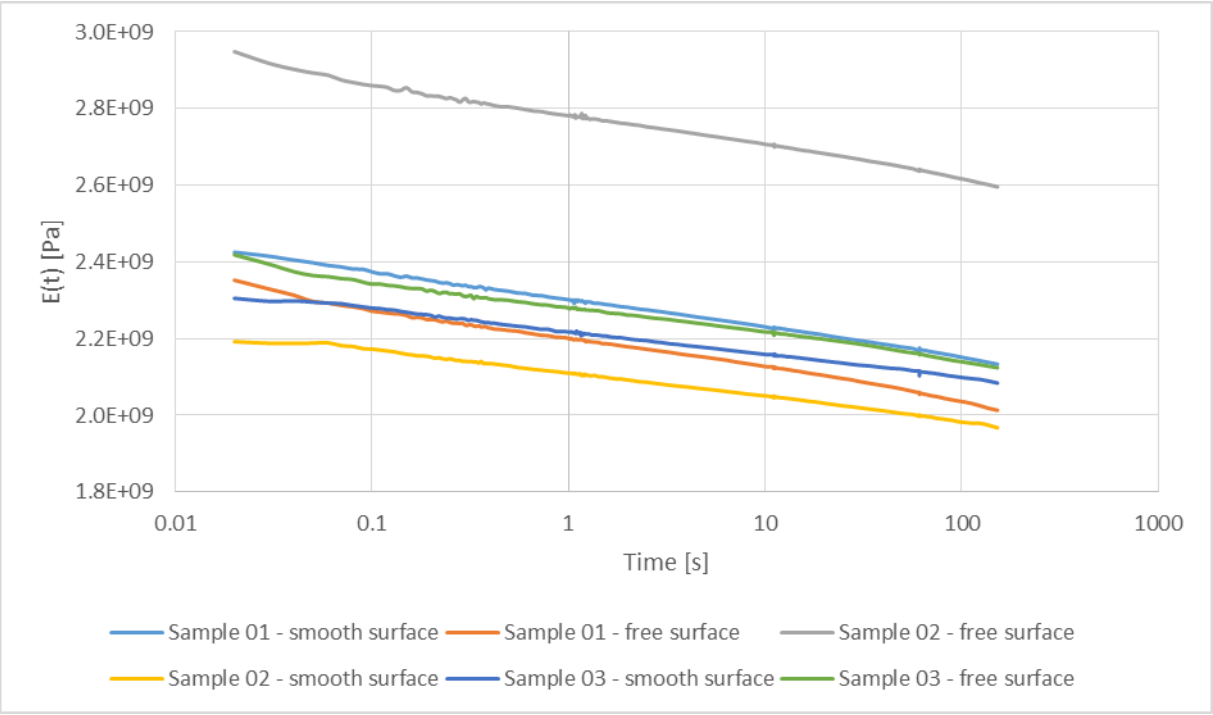

Figure 24 – Comparison of relaxation modulus obtained for different samples at ambient temperature

These relatively short tests allow a better selection of the sample to test at different temperatures, based on similarities between the curves despite the tested surface. Both samples 01 and 03 show a good correlation between values, thus sample 01 was chosen.

Compressed air is used to control the temperature. This limited the lowest temperatures at which it was possible to perform tests to the temperature of the machine's house where the compressor that provides the air is located.

According to the EPOLAM 2025 data sheet (APPENDIX A), the glass transition temperature is at 135°C. However, for safety reasons the maximum value up to which the resin is tested is 100°C and the results are as shown in Figure 25, Figure 26 and Figure 27.

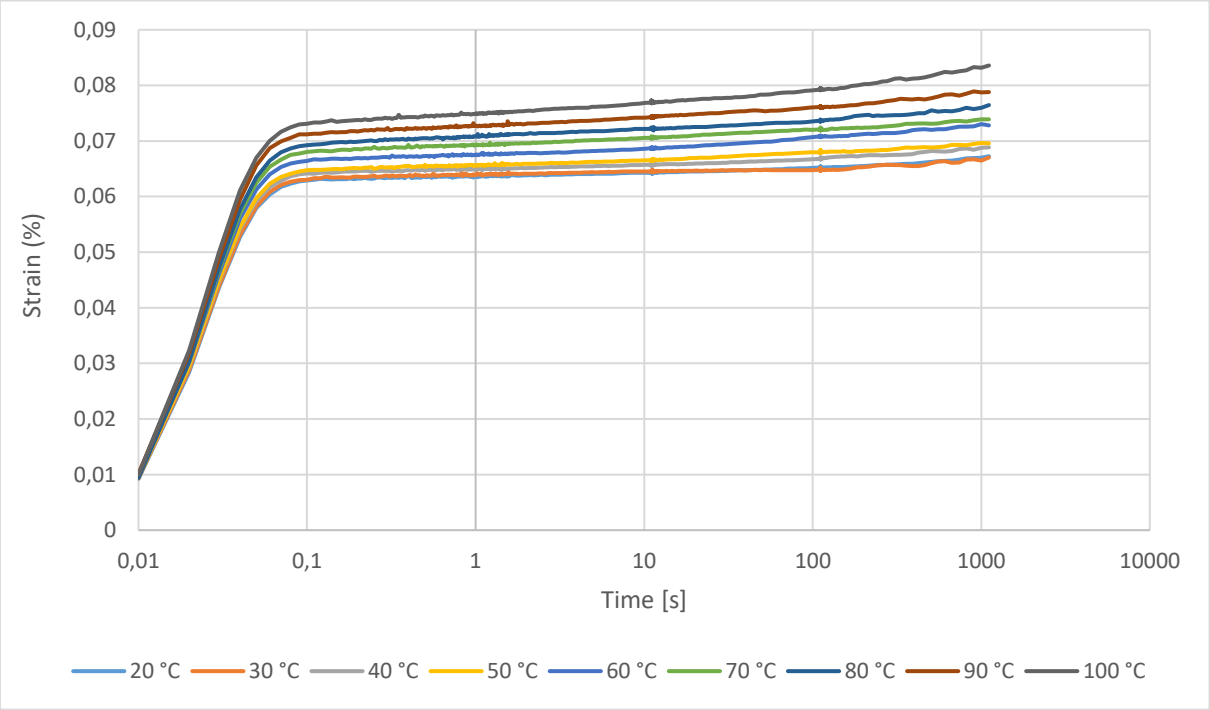

Figure 25 – Imposed strain in controlled temperature viscoelastic relaxation tests

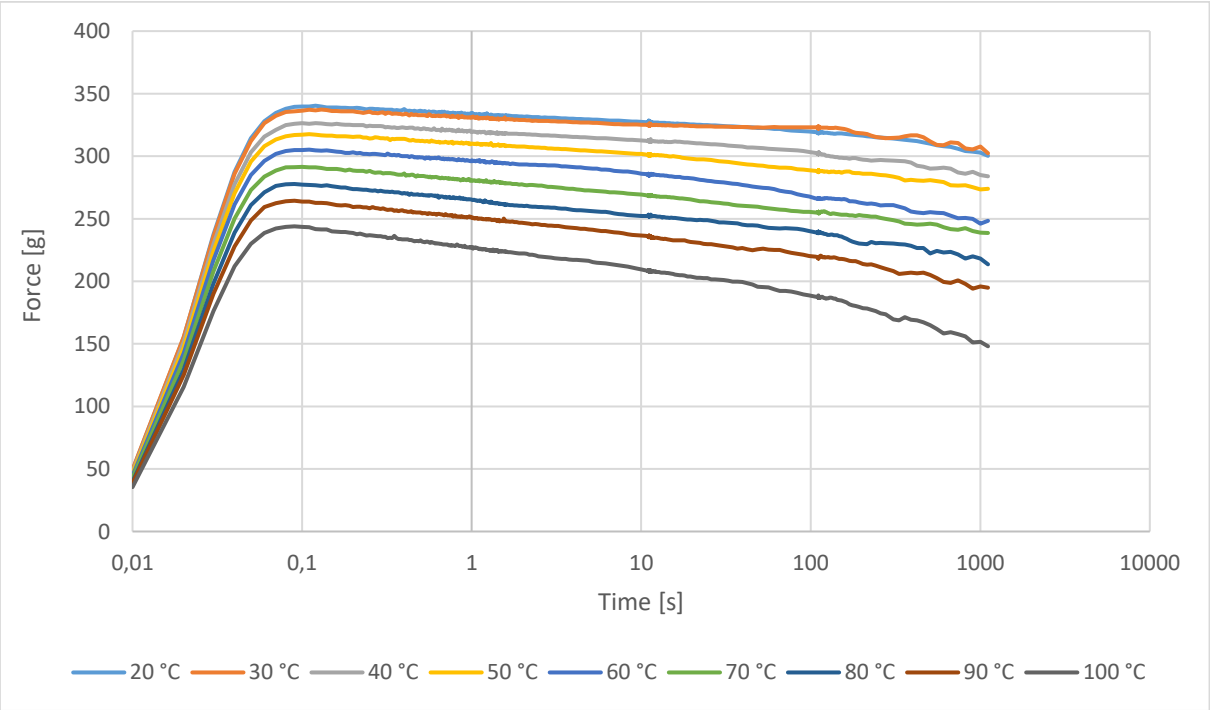

Figure 26 – Input values of force for controlled temperature viscoelastic relaxation test

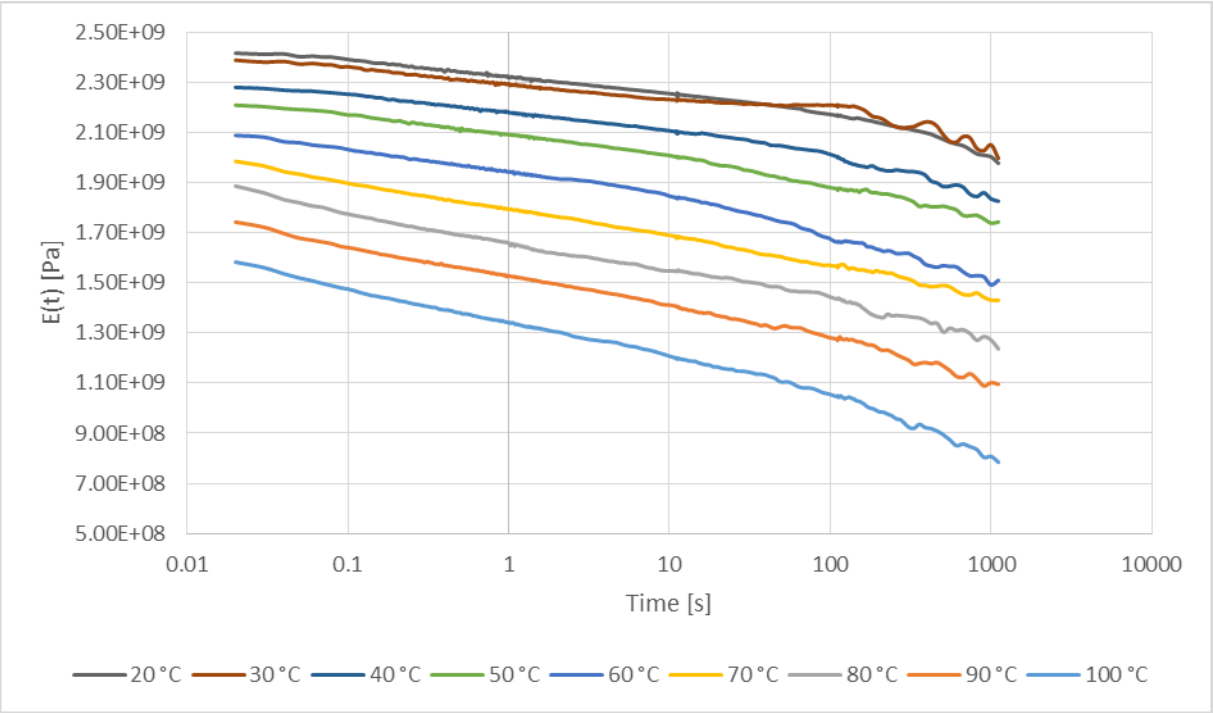

Figure 27 – Relaxation tests performed at different temperatures

It is possible to observe how little the relaxation modulus changes between 20 and 30°C, implying a stable behaviour up to these temperatures. This validates the possibility of using linear elastic considerations for such temperatures, as the variations suffered by the modulus can be disregarded without greater influence in the outcome results.

The curves are fit to be overlapped as they all share common values with the previous and following curve. The master curve that results from applying the TTS is plotted in Figure 28. It is represented by the considered Arrhenius fit – equation 2.31, where E_a represents the apparent activation enthalpy and r^2 the coefficient of determination of the fitting. A smoother version of this curve is presented in Figure 29. The curves were approached by a Prony series with the terms presented in Table 1.

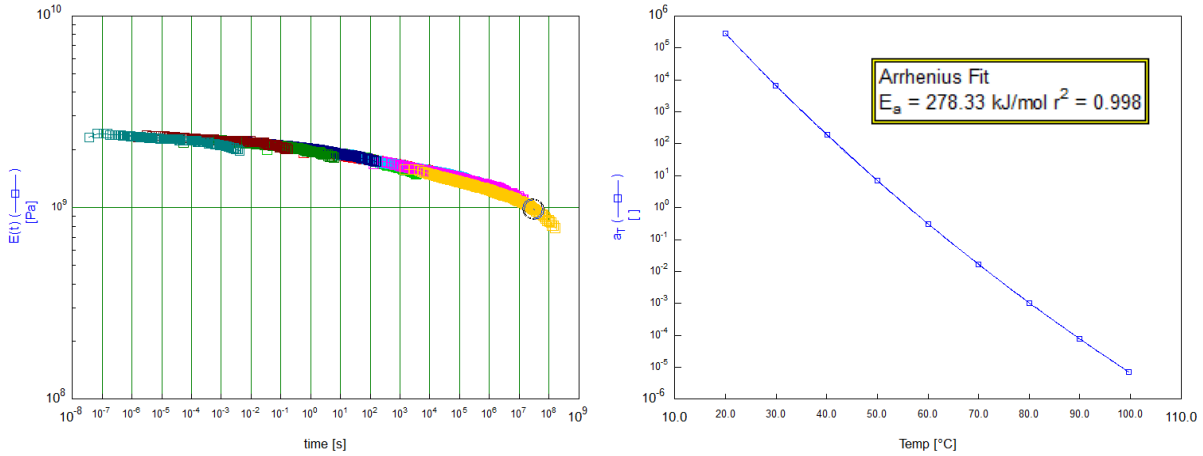

Figure 28 – TTS principle with overlapped temperature curves and respective Arrhenius fit

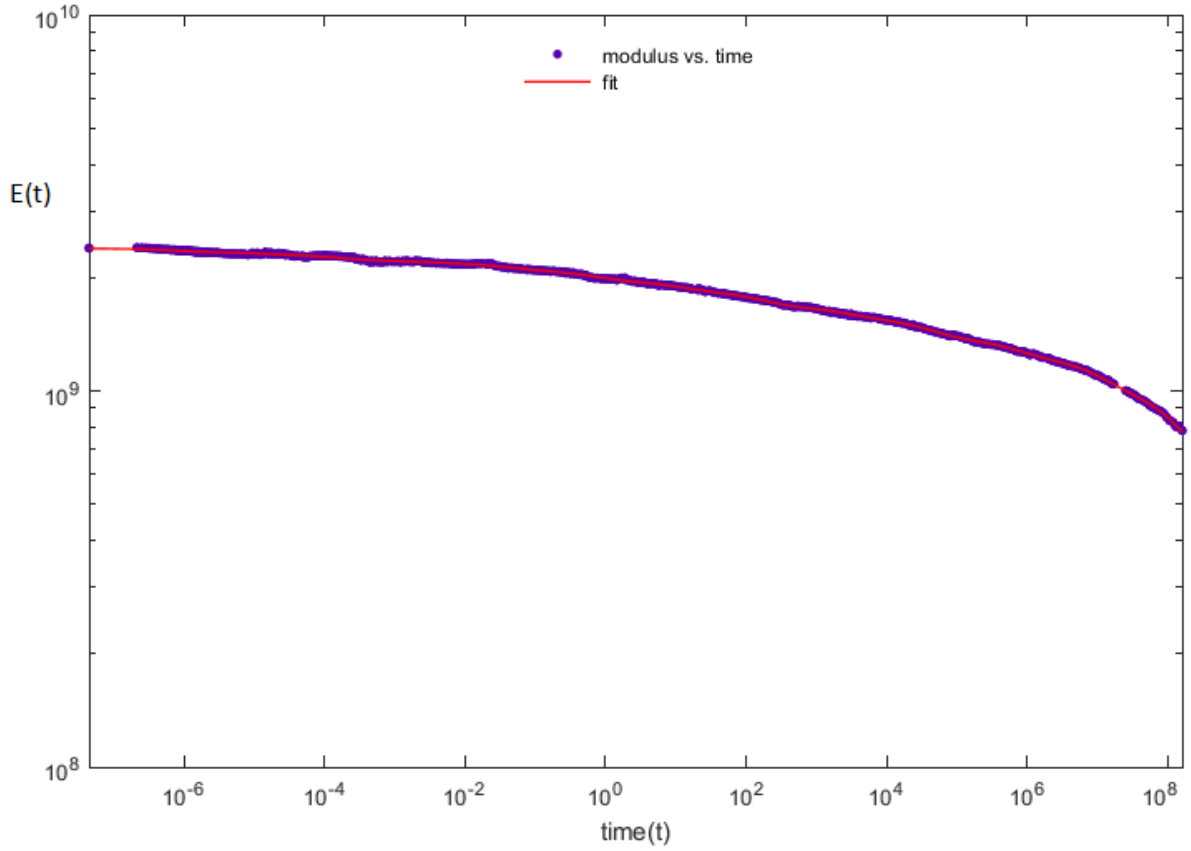

Figure 29 – Relaxation modulus' master curve and respective Prony series fit

Table 1 - Terms of the Prony series that fits the TTS master curve

$\tau_i\ [s]$	e_i
$\tau_1 = 7.037 \times 10^{-7}$	$e_1 = 2.2 \times 10^{-2}$
$\tau_2 = 1.106 \times 10^{-5}$	$e_2 = 1.28 \times 10^{-2}$
$\tau_3 = 1.737 \times 10^{-4}$	$e_3 = 3.61 \times 10^{-2}$
$\tau_4 = 2.73 \times 10^{-3}$	$e_4 = 1.31 \times 10^{-2}$
$\tau_5 = 4.29 \times 10^{-2}$	$e_5 = 3.72 \times 10^{-2}$
$\tau_6 = 6.74 \times 10^{-1}$	$e_6 = 5.39 \times 10^{-2}$
$\tau_7 = 10.59$	$e_7 = 4.9 \times 10^{-2}$
$\tau_8 = 166.4$	$e_8 = 7.11 \times 10^{-2}$
$\tau_9 = 2615$	$e_9 = 4.64 \times 10^{-2}$
$\tau_{10} = 4.109 \times 10^{4}$	$e_{10} = 7.63 \times 10^{-2}$
$\tau_{11} = 6.456 \times 10^{5}$	$e_{11} = 6.06 \times 10^{-2}$
$\tau_{12} = 1.014 \times 10^{7}$	$e_{12} = 8.54 \times 10^{-2}$
$\tau_{13} = 1.594 \times 10^{8}$	$e_{13} = 1.76 \times 10^{-1}$
$E_0 = 2.397 \times 10^{9}\ Pa$	
$R^2 = 0.99957$	

A considerable difference is noticed between E_0 and the Young's modulus calculated in Table 1. This happens as a result of several influences of the specimen geometry, material fabrication process, type of loading, mathematical considerations and even measuring equipment. For the tensile test, the linear fitting of the elastic behaviour may not be the most precise (a higher R^2 parameter can be chosen), the load cell or the extensometer may not be properly calibrated; for the relaxation test, since it is done for flexure, a very detailed measure of the thickness t must be done because that parameter highly affects the inertial moment in the test direction, equation 4.1. The fabrication process may also alter the uniformity of the material's properties, as it is poured in a container and no information is known about the drying process, but residual stresses may arise from temperature gradients and affect the final results. The machining process may affect more the 3-PTB specimen than the dogbone, as it is smaller.

$$I = \frac{1}{12} b \cdot t^3 \tag{4.1}$$

4.2 Tensile test results

The tensile tests give important information about failure parameters, suitable to be used as generalized parameters in the generalized local model. Out of the possibilities (stress, strain, energy released, displacement or force), the ultimate tensile strength along the loaded axis is one important parameter that is chosen as GP for the probabilistic analysis to be performed in this section. In particular, the PFCDF associated with the ultimate tensile strength will be evaluated. The tensile strength is used as a reference and its suitability can be easily assessed in the probabilistic model. Different choices of GP, which can ultimately be done with the data provided in this work can also be proposed. Although, as it goes beyond the scope of the project, it is only mentioned as future work.

The tensile tests were performed in twenty five specimens and retrieved each material force vs. displacement plot – Figure 30. The corresponding maximum stresses and strains are represented in Table 2.

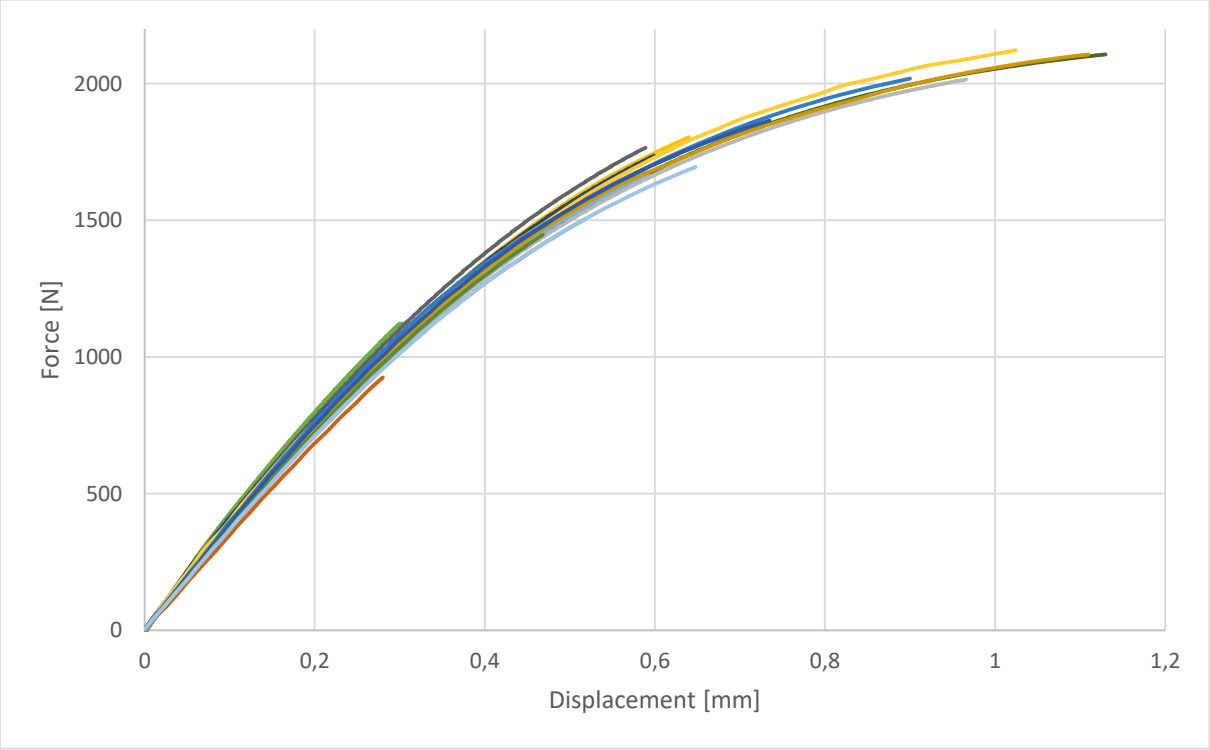

Figure 30 – Force vs displacement curves of all tensile tests

The two first tests are disregarded – Table 2 – as the first does not fulfil the stipulated displacement rate and the second was performed without the extensometer attached; the stress values could still be used as generalized parameters as neither of the events directly affects the outcome. However, to be able to compare specimens under the closest conditions as possible, they are not considered.

Table 2 - Tensile test results

Specimen	Ultimate Tensile Strength [MPa]	Maximum Strain (%)	Young's Modulus [GPa]
E22-8	65.2	3.5	Disregarded
E22-2	61.5	-	Disregarded
E22-12	69.3	2.9	3.7
E18-1	74.1	3.2	3.8
E18-11	71.5	3.1	3.2
E18-4	45.4	1.6	Disregarded
E18-9	49.4	1.7	3.3
E18-7	69.9	2.9	3.2
E22-6	71.0	2.9	3.3
E28-8	67.8	3.0	3.3
E22-11	70.7	3.0	3.4
E28-10	87.6	5.7	3.2
E28-11	70.8	3.0	3.4
E22-9	57.8	2.1	3.2
E28-7	85.5	4.8	3.2
E22-7	86.0	5.1	3.2
E22-1	73.2	3.1	3.2
E28-1	68.0	2.7	3.2
E28-4	83.4	4.5	3.2
E22-4	39.9	1.4	Disregarded
E28-6	66.9	2.6	3.2
E28-2	87.8	5.6	3.1
E28-5	81.1	3.7	3.3
E28-9	62.9	2.3	3.1
E28-12	77.7	3.2	3.3
Mean values	73.0	3.3	3.2
Std Dev	9.9	1.1	0.07

The specimens presented a brittle behaviour, with no notorious plastic deformation in the section where they fail – Figure 31.

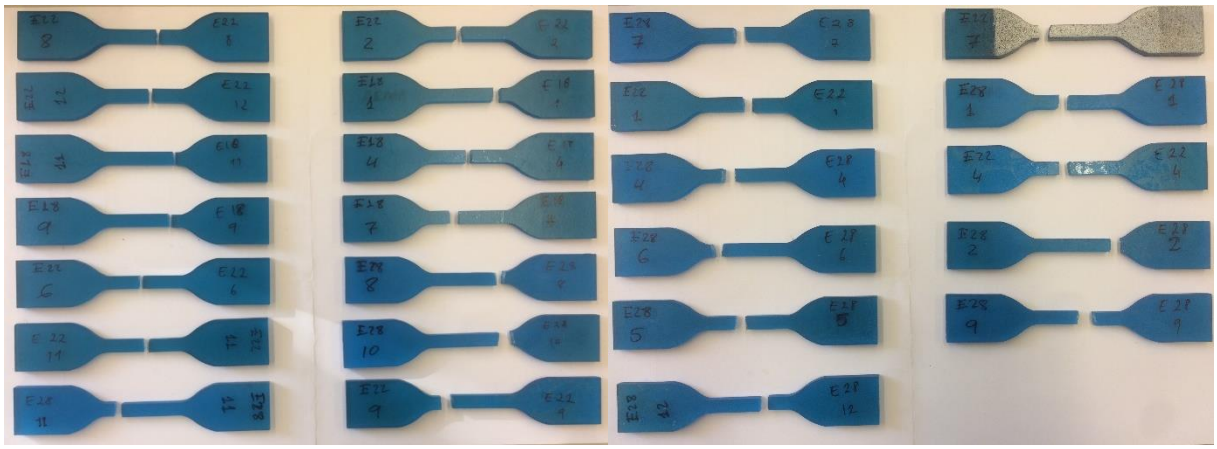

Figure 31 – Specimens after tensile test

The first step to evaluate the remaining data from the tensile tests was to analyse the specimens which break with lower load values and are wide apart from the average. That is the case of E18-4, E18-9 and E22-4, which have the lowest registered ultimate tensile strengths. In specimen E18-4 a surface notch caused by an air bubble is noticeable – Figure 32 – and assumed as the main reason for the rapid failure, specimen E22-4 presented a similar notch and both are disregarded. In specimen E18-9 there is no notorious reason for such a low stress so it is considered a valid experimental test.

Figure 32 – Aspect of the E18-4 specimen rupture, presenting a notch

The influence of the sheets from where the samples are taken is questioned. However, as the populations are rather small – three for the E18 and five for the E22 – the mean values per sheet are not considered representative of differences in behaviour. Taking the E18 sheet, for instance, such a small population is going to be largely affected by a single value like it happens when considering the E18-9, a representation of this effect is shown in Table 3.

x

Table 3 - Influence of a single parameter considering data from single sheets, the case of E18 sheet

	E18 sheet	
	Considering E18-9 specimen	Disregarding E18-9 specimen
Average	66.2 MPa	71.9 MPa
Std Dev	11.3 MPa	2.1 MPa

Specimen E22-7 was analysed using DIC to determine the Poisson's coefficient of the material. The DIC analysis allowed to obtain both longitudinal and transversal deformation – APPENDIX C – from which the values corresponding to the linear behaviour region were chosen. The selection process consisted on determining the coefficient of determination between the axial stress and the longitudinal deformation and assuming the material behaves linearly as long as the coefficient is within a defined range of $0.998 \leq R^2 \leq 1$. Selecting the deformations associated with the values that falls under the selected range, applying equation 3.3 and calculating their arithmetic mean, it is possible to calculate Poisson's coefficient that returned the value of 0.36.

A numerical simulation is performed to validate a numerical model – Figure 33 – using specimen E28-2, which showed the highest ultimate tensile strength. The material is defined as elastoplastic. Its behaviour at ambient temperatures is proven to exhibit low viscous effect (section 4.1). The Young's modulus E and Poisson's ratio ν of 3.238 GPa and 0.36, were respectively adopted. The parameters for the plastic characterization are shown in APPENDIX D in the form of a stress-plastic strain table.

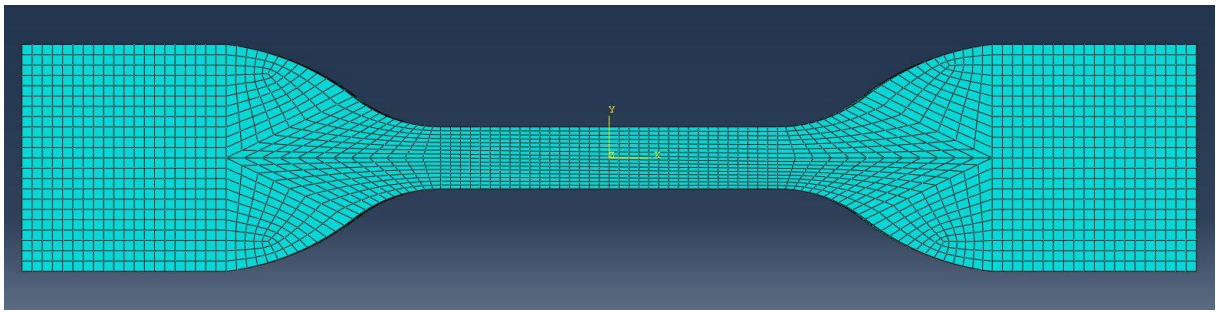

Figure 33 – Dogbone specimen numerical simulation mesh

The model is submitted to a very high displacement and tested until the limit of its elastoplasticity. This tries to recreate the moment prior to failure and allows an evaluation and comparison of the model up to that point with the experimental stress-strain curve.

A constant axial stress is obtained along the gauge section – Figure 34. The stress-strain curve is obtained directly in *ABAQUS*™ by selecting the values in a random element of the neck section, as they all present the same values. The stress-strain curve – Figure 35 – is plotted versus the true stress-strain curve of the experimental results and compared to it. The results from numerical simulation show a good coherence and differences small enough not to be taken into account – all the errors are under 2.5%. This implies that the model is correctly defined in terms of the material parameters and the same definitions are suitable of being used to characterize other type of geometries from the same material.

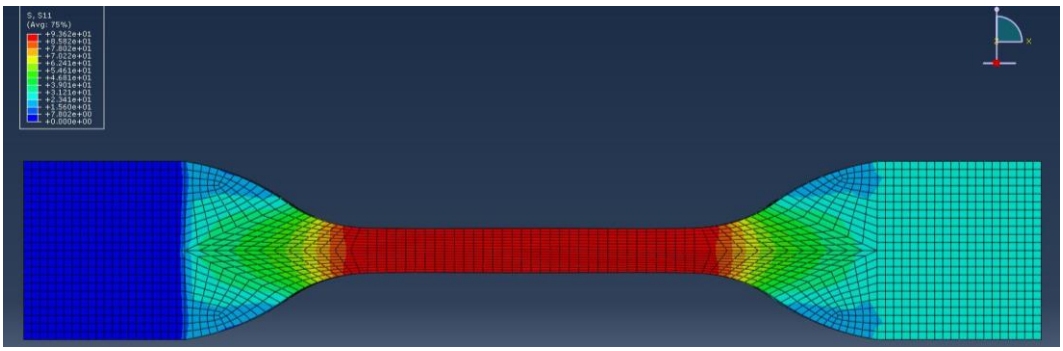

Figure 34 – Axial stress output of dogbone specimen

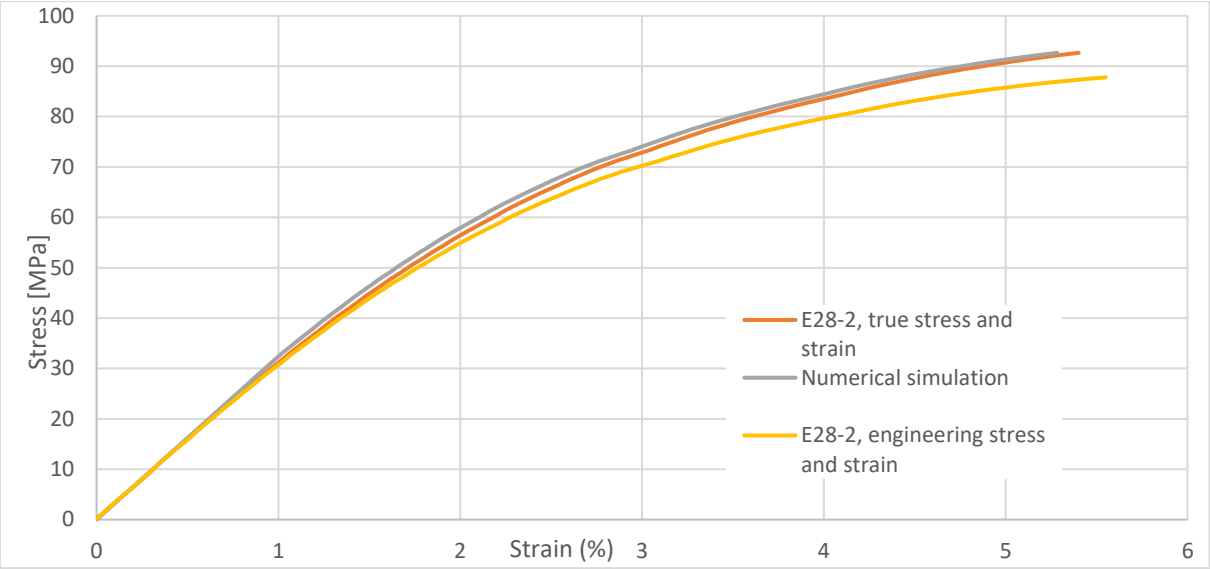

Figure 35 – Stress-strain curves for E28-2, with true and engineering data, and for numerical simulation

4.3 Compact tension test results

Compact tension specimens are tested without a crack, using only the machined notch. The decision of not inserting a crack has to do with the high brittleness of the material, as it makes it hard to use traditional cracking methodologies without disabling the specimen, making it inappropriate for further testing. As the method in study (GLM) does not rely on the geometry (in the sense that it can be applied to any geometry), this issue should not affect the outcome results of the probabilistic study developed afterwards.

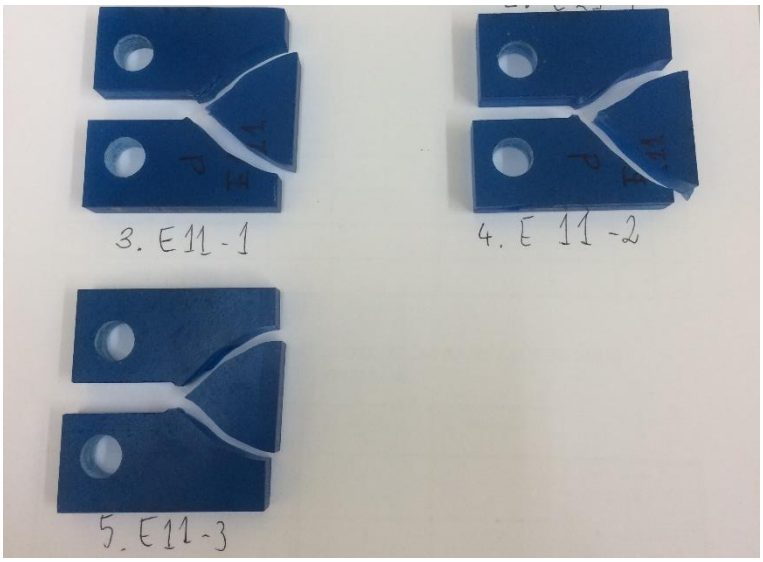

Figure 36 – CT specimens after failure

Three specimens were loaded axially until failure – Figure 36 – and the force applied values were recorded – Table 4. There was no record of the crack opening displacement (COD) or any other displacement criteria while performing the tests as it was impractical to use extensometers and DIC apparatus was not available at the time the tests were performed. This may affect the outcome, as there is no experimental data besides the force to be considered and tested numerically and the stress field is too complex to be obtained directly, around the notch tip.

Table 4 - CT specimen experimental results

Specimen	Max Load [N]
E11 – 1	1131
E11 – 2	1037
E11 – 3	1299
Mean values	1156
Std Dev	133

A numerical model was elaborated for the CT specimen – Figure 37 – using the same material properties as previously defined in section 4.2 for the tensile test and considering plane stress for a thickness of 10 mm. This consideration assumes a constant stress along the thickness. Despite material's brittleness and a close to linear failure on the specimens after being tested – Figure 36 – this consideration must be used with some reservations as some specimens present visible internal defects – Figure 38 – that may alter the stress distribution along the thickness of the specimen.

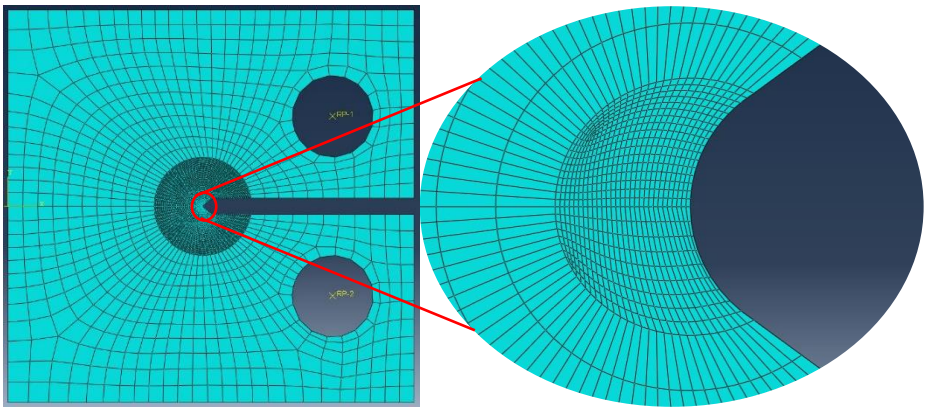

Figure 37 – CT specimen numerical simulation mesh

Figure 38 – CT specimen showing internal defects

A numerical simulation was performed for 1,500N, as it is a value higher than any of the presented and should ensure that the resulting stresses calculated are in the edge of the elastoplastic behaviour of the CT specimen. The direct stress along the loading direction obtained using this numerical model is shown in Figure 39.

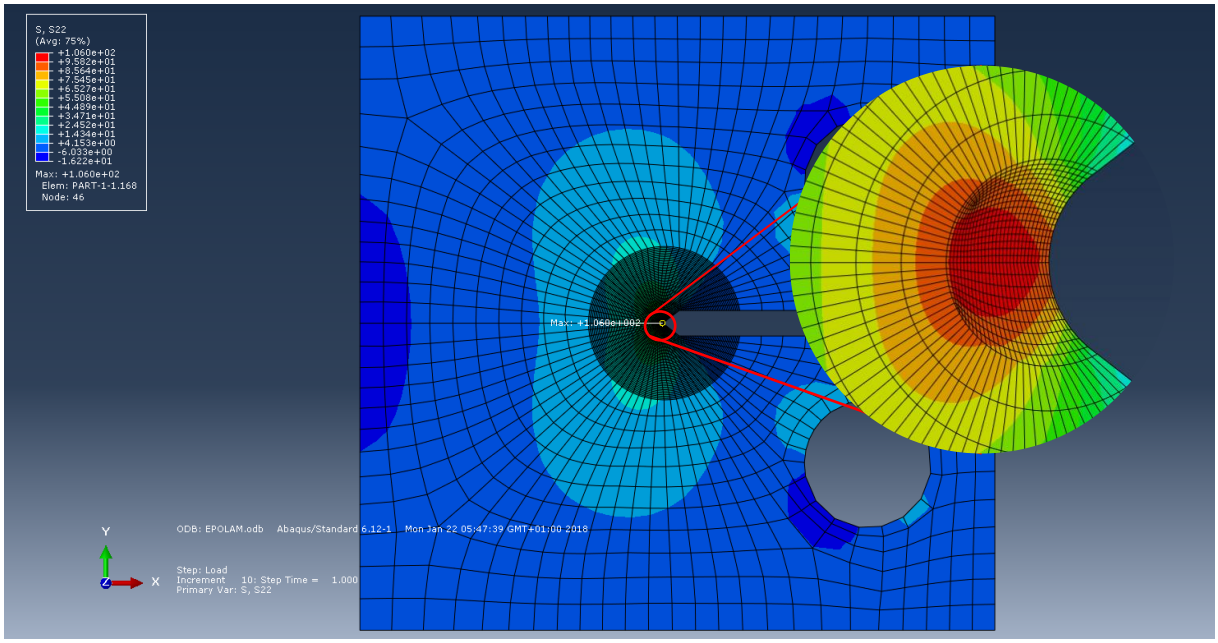

Figure 39 – Distribution of the direct stress along the loading direction, across the CT specimen

4.4 Probabilistic assessment of results

Considering the tensile tests experimental data and applying Bernard's formula – equation 2.42 – to the chosen GP of ultimate tensile strength as shown in Table 2, it is possible to obtain an expected probability of failure P_f associated with each of the GP values – Table 5.

Table 5 – Probability of failure corresponding to generalized parameters of ultimate tensile strength

GP – Max Stress[MPa]	P_f (%)
49.428	0.03271
57.783	0.079439
62.937	0.126168
66.935	0.172897
67.821	0.219626
68.007	0.266355
69.317	0.313084
69.907	0.359813
70.693	0.406542
70.821	0.453271
70.983	0.5
71.513	0.546729
73.175	0.593458
74.136	0.640187
77.658	0.686916
81.106	0.733645
83.404	0.780374
85.472	0.827103
86.018	0.873832
87.602	0.920561
87.774	0.96729

A *MATLAB*® script is used to perform linear regressions considering location parameters λ from the range shown in equation 5.1. The coefficient of determination R^2 is used to assess which linear regression better fits the data and then returns the λ corresponding as well as the estimation value – Figure 40.

$$0.5 \cdot GP_{min} \leq \lambda \leq 0.9999 \cdot GP_{min} \tag{5.1}$$

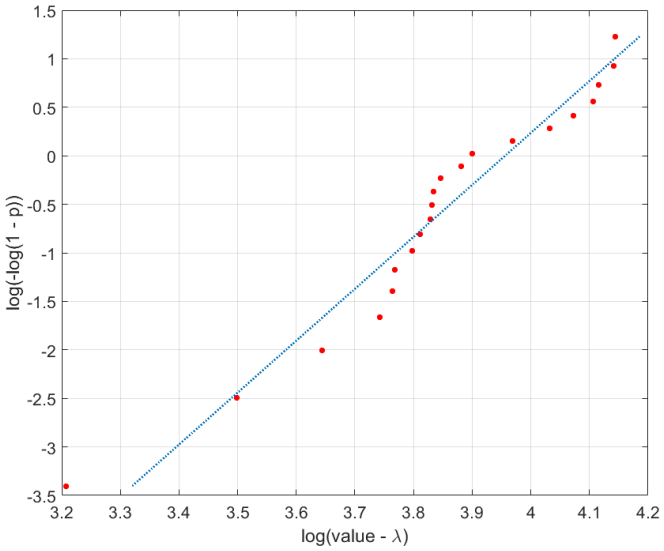

Figure 40 – Linear regression associated with the best fit for a location parameter λ

Applying equations 2.45 to 2.48 to this linear regression, it is possible to calculate all three of the Weibull's cdf parameters that generate the EFCDF. Having the parameters calculated, the EFCDF is plotted for an equivalent size of $792mm^3$ – Figure 41. This size is taken from the rectangular cross-section of the dogbone (33x6x4 mm) assuming a constant generalized parameter along this gauge section. The consideration of uniform GP is proved by the stress distribution in the numerical simulation – Figure 34.

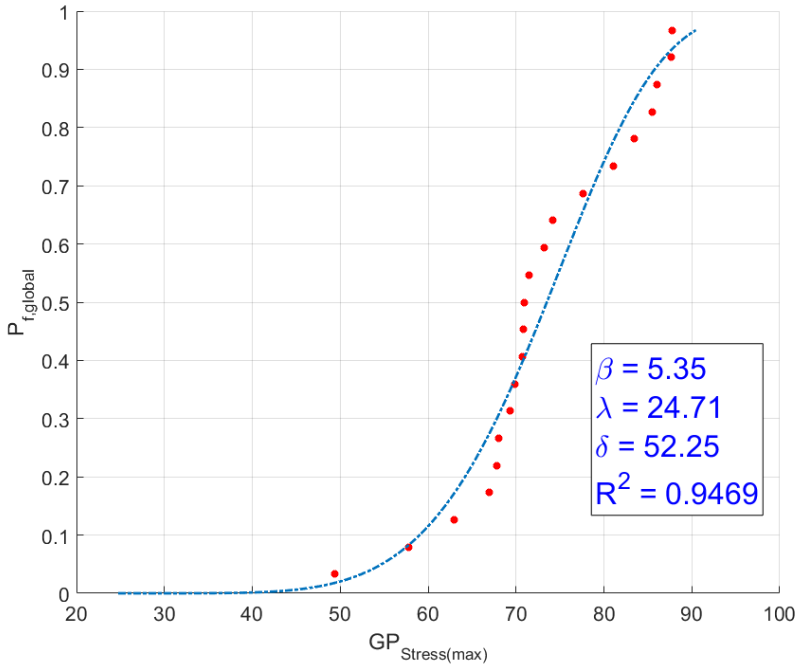

Figure 41 – Experimental failure cumulative distribution function, its Weibull parameter and coefficient of determination for the tensile test

The distribution of the GP using Bernard's formula has a Weibull's cdf fitting that is not optimal. There is a high concentration of values around the right-side tail that shift the cdf. Despite this fact, R^2 is still high enough to say that the location parameter is valid and that the EFCDF is a good approach to the experimental data. More tests should be performed, out of the same sheet and from several sheets to assess their influence.

The Weibull parameters to fit a reference size $S_{ref} = 1mm^3$ can now be easily calculated through a *MATLAB*® function. Substituting them into equation 2.49, derives the material's PFCDF, which is represented in Figure 42. The weakest link principle is verified as with a decrease of the considered volume, there is a lower probability of existence of a defect leading to failure and, therefore, a lower probability of failure which, in the end, translates into higher resistance.

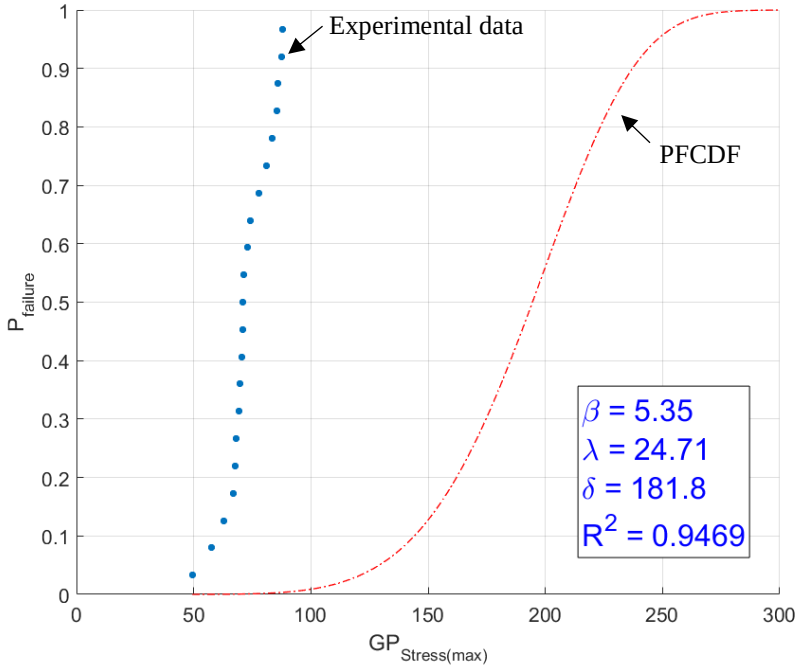

Figure 42 – Primary failure cumulative distribution function, for a reference size of $1mm^3$

Having a valid and verified numerical model is a great complement to the Generalized Local Model because it is possible to obtain the volumes of the elements used in the mesh of the FEM analysis. Using refined meshes, it is possible to assume a constant distribution of the generalized parameter in an element without introducing a considerable error. This makes the GLM applicable to any type of geometry, regardless of its complexity.

To test this functionality, the reverse process is going to be performed. This is done by deriving the EFCDF of the tensile specimen from the obtained PFCDF, applied to the tensile test numerical model and considering its elements of volume. Then, the same is performed for the CT specimens.

For this type of numerical simulation, ten equally spaced load steps are considered and the probability of failure is to be computed for each of the increases. The probability of failure is calculated for every element of the model's mesh with an equivalent size equal to the original, non-deformed, element.

The *ABAQUS*™ input file, containing the field output of stresses and elements' volumes, is loaded into *Abaqus2matlab* and those values exported to *MATLAB*® through it.

A global probability of failure is calculated using Weibull's parameters for the reference size of $1mm^3$, using each elements volume as equivalent size S_{eq}. Applying the weakest link

principle to each of these probabilities, returns the global probability of failure of the tensile test specimen – Figure 43. The same process was performed for the compact test – Figure 44 – which was compared with stress values calculated by applying the resulting force from the test (as shown in Table 5) to the numerical model.

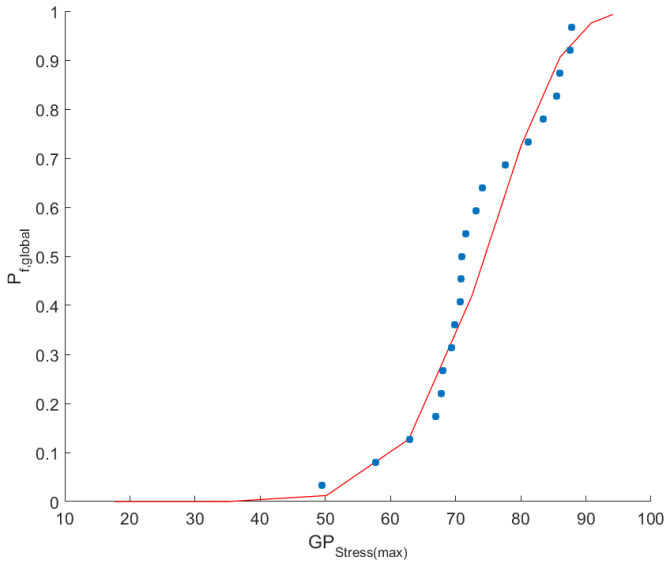

Figure 43 – Global probability of failure for a tensile test numerical model, derived from the PFCDF, and compared with experimental data

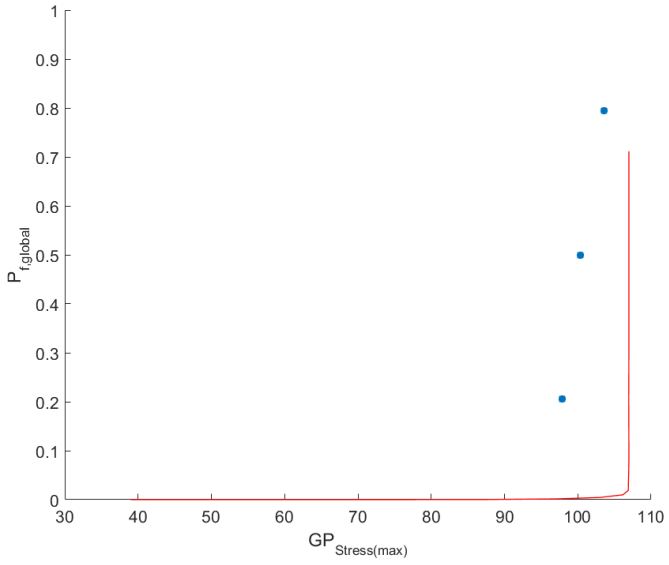

Figure 44 – Global probability of failure for a compact tension test numerical model, derived from PFCDF, and compared with computed data

The curve associated with the global probability of failure, derived from the PFCDF – Figure 43 – presents obvious similarities with the obtained EFCDF – Figure 42 – and a similar correlation with the experimental data. It is possible to assume that, given a higher number of load steps, the curves would overlap.

For the compact tension model, however, the global probability of failure associated did not even displayed up to a value of nearly 1. To determine what might have caused such error, some alterations of the *MATLAB*® script were made, adjustments to the *ABAQUS*™ numerical model and queries about its elements.

As the best location parameter determined is equal to the minimum value considered (0.5 times the minimum GP) - Figure 42, it is possible that the imposed limit is stopping a better parameter to be achieve and, as so, a new range of values was considered with zero contained – $0 \leq \lambda \leq 0.99 \cdot GP_{min}$. This returns a slightly better approach to the location parameter value and different Weibull's parameters. The EFCDF was calculated, as well as the PFCDF – APPENDIX E. However, when the fit to the CT specimens' data is applied there are not significant improvements.

The numerical simulation's mesh was redefined and the number of elements increased – Figure 45 – to assess its influence on the final results but there were no notorious differences. Also, additional frames and calculation steps were considered but with the same, non-effective, outcome – Figure 46.

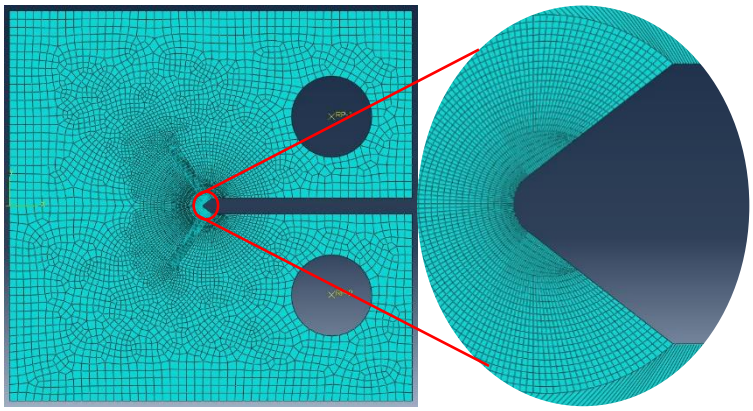

Figure 45 – Redefined mesh for the CT numerical model with an additional number of elements

As the stress only slightly changes with each increment of force, a high increment taking into account the experimental data, it is deductible that the cross-section area is lengthening almost proportionally to the force increase. Such is normal due to the high plastic deformation suffered in the notch. Opting for a generalized parameter of maximum axial load, it is possible to better assess its influence on the solution – Figure 47 – and it calls into question if the use of stress as an appropriate generalized parameter for this specific case.

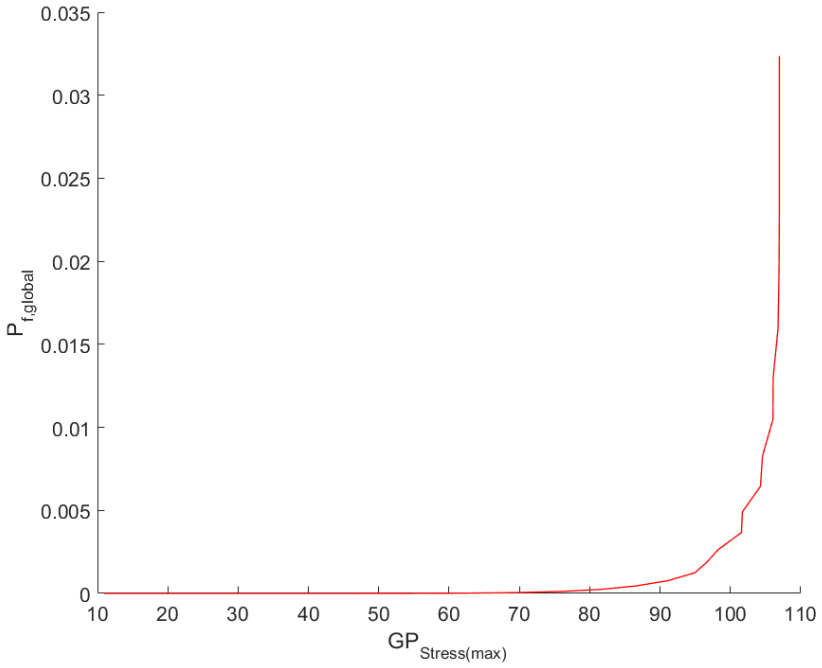

Figure 46 – Output curve of the GLM applied to CT geometry, with a maximum load of 2,000N (25 load steps) and a refined mesh

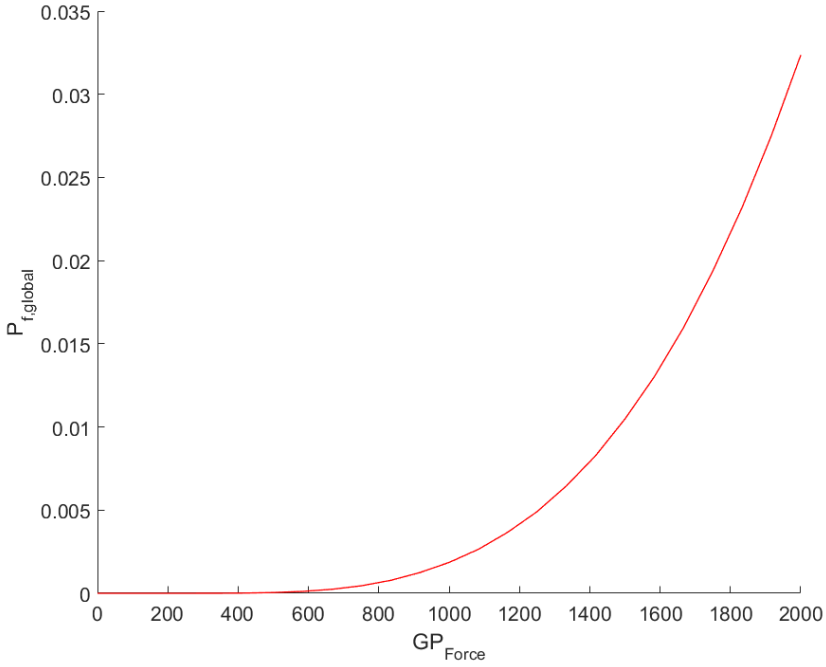

Figure 47 – Output curve of the GLM applied to CT geometry, with a maximum load of 2,000N (25 load steps) and a refined mesh, considering force as GP

5 Conclusions

The main objective of this dissertation was to assess the suitability of applying the Generalized Local Model to a commercial epoxy resin – EPOLAM 2025, in particular to characterize its mechanical strength.

A viscoelastic characterization was performed to inquire the material's mechanical behaviour, under the influence of time and temperature. The material was found stable at ambient temperatures, up to 30℃, without major changes in its relaxation modulus. The linear elastic similarities in behaviour are verified in tensile tests performed after, within the considered temperatures.

The tensile tests were performed according to ASTM D638 (2004) and an elastoplastic behaviour with high degree of brittleness was observed. The results show high scatter of the considered generalized parameter, the ultimate tensile strength – ranging from 49 MPa to 87 MPa, with an average value of 73 MPa. The material Poisson's ratio was evaluated using digital image correlation and was found equal to 0.36.

A numerical finite element model based on the experimental data gathered from the tensile tests was elaborated and showed a good correlation between numerical and experimental stress-strain curves.

The generalized local model was used for the tensile tests data and an experimental failure cumulative distribution function (EFCDF) was obtained. The material's primary failure cumulative distribution function was derived from the experimental failure cumulative distribution function (PFCDF) for a reference size of $1mm^3$.

The model validation trial was made by using compact tension (CT) tests' experimental data. The stresses were calculated using a FE numerical model, with a material model calibrated with the tensile specimen. The outcome EFCDF does not fit the cumulative distribution function derived from the PFCDF applied to the reference size of a CT specimen. As such, the applicability of the generalized local method was unsuccessful.

5.1 Future works

ARAMIS CDI should be used in the CT tests to compute the crack tip opening displacement. That same displacement ought to be applied in the numerical analysis and the force output compared with the one obtained in the experimental test, or applying a force and comparing the displacement, in order to assess the numerical model.

Also, as only three CT specimens were tested, it is possible that the calculations are correct but, by chance, the failure happened in situations of low probability. A higher population should be considered, as well as different geometries.

Different generalized parameters should be tested and the results compared with the ones obtained in this work, such as the strain based parameters.

References

ASTM. 2001. “ASTM D5023-01: Standard Test Method for Plastics: Dynamicac Mechanical Properties: In Flexure (Three-Point Bending). ” *ASTM International*. https://doi.org/10.1520/D5023-01.

ASTM. 2004. “ASTM D638-03: Standard Test Method for Tensile Properties of Plastics.” *ASTM International*. https://doi.org/10.1520/D0638-03.

Beremin, F. M., A. Pineau, F. Mudry, J. C. Devaux, Y. D’Escatha, and P. Ledermann. 1983. “A Local Criterion for Cleavage Fracture of a Nuclear Pressure Vessel Steel.” *Metallurgical Transactions A* 14 (11):2277–87. https://doi.org/https://doi.org/10.1007/BF02663302.

Bernard, A., and E.C. Bosi-Levenbach. 1953. “The Plotting of Observations on Probability Paper.” *Statististica Neederlandica*, no. 7:163–73. https://doi.org/10.1115/1.3256391.

Blasón, S., M. Muniz-Calvente, R. Koller, C. Przybilla, and A. Fernández-Canteli. 2017. “Probabilistic Assessment of Fatigue Data from Shape Homologous but Different Scale Specimens. Application to an Experimental Program.” *Engineering Fracture Mechanics*. https://doi.org/10.1016/j.engfracmech.2017.05.017.

Boltzmann, L. 1876. “Zur Theorie Des Elastischen Nachwirkung.” *Pogg. Ann. Phys* 227 (1):108–19. https://doi.org/10.1002/andp.18742270106.

Bonifasi-Lista, Carlos, Spencer P Lake, Michael S Small, and Jeffrey A Weiss. 2005. “Viscoelastic Properties of the Human Medial Collateral Ligament under Longitudinal, Transverse and Shear Loading.” *Journal of Orthopaedic Research : Official Publication of the Orthopaedic Research Society* 23 (1):67–76. https://doi.org/10.1016/j.orthres.2004.06.002.

Bott, R. 2014. *Computational Viscoplasticity*. *Igarss 2014*. https://doi.org/10.1007/s13398-014-0173-7.2.

Calvente, Miguel Muñiz. 2017. “The Generalized Local Model: A Methodology for Probabilistic Assessment of Fracture under Different Failure Criteria.”

Castillo, E. 1988. *Extreme Value Theory in Engineering*. New York: Academic Press.

Castillo, Enrique, Alfonso Fernandez Canteli, Volker Esslinger, and Bruno Thurlimann. 1985. “Statistical Model for Fatigue Analysis of Wires, Strands and Cables,” 1–40.

Cocco, R. G., P. M. Frontini, and J. E. Perez Ipiña. 2007. “Threshold Toughness of Polymers in the Ductile to Brittle Transition Region by Different Approaches.” *Engineering Fracture Mechanics* 74 (10):1561–78. https://doi.org/10.1016/j.engfracmech.2006.09.011.

Correia, José A.F.O., Abílio M.P. De Jesus, and Alfonso Fernández-Canteli. 2013. “Local Unified Probabilistic Model for Fatigue Crack Initiation and Propagation: Application to a Notched Geometry.” *Engineering Structures* 52 (April 2015):394–407. https://doi.org/10.1016/j.engstruct.2013.03.009.

Doolittle, A. K. 1951. “Studies in Newtonian Flow. 1. The Dependence of the Viscosity of Liquid on Temperature.” *Journal of Applied Physics* 22:1031–35.

Drozdov, Aleksey D. 1998. *Mechanics of Viscoelastic Solids*. Wiley. http://as.wiley.com/WileyCDA/WileyTitle/productCd-0471975125.html.

Fernández, Pelayo. 2011. “Métodos de Conversión Tiempo-Frecuencia Para La Aplicación Del Principio de Correspondencia En Materiales Viscoelástico-Lineales.” *Anales de Mecánica de La Fractura 28* 2:243–48.

Ferry, Door John D. 1980. *Viscoelastic Properties of Polymers*. 3rd ed. John Wiley & Sons.

Ferry, John D. 1980. *Viscoelastic Properties of Polymers*. *New York: Wiley*. https://doi.org/10.1016/0010-4361(73)90801-X.

Findley, W.N. 1978. *Creep and Relaxation of Nonlinear Viscoelastic Materials*. *Polymer*. Vol. 19. https://doi.org/10.1016/0032-3861(78)90187-8.

García Prieto, María Antonia. 2001. "Dimensionamiento Probabilístico Y Análisis Experimental de Vidrios En Rotura." Universidad de Oviedo.

Gündoğdu, Ö. 2007. "Optimal Seat and Suspension Design for a Quarter Car with Driver Model Using Genetic Algorithms." *International Journal of Industrial Ergonomics* 37 (4):327–32. https://doi.org/10.1016/j.ergon.2006.11.005.

Herbert, R. D., A. M. Moseley, J. E. Butler, and S. C. Gandevia. 2002. "Change in Length of Relaxed Muscle Fascicles and Tendons with Knee and Ankle Movement in Humans." *Journal of Physiology* 539 (2):637–45. https://doi.org/10.1113/jphysiol.2001.012756.

ISO 13586, BS. 2000. "Plastics — Determination of Fracture Toughness (G IC and K IC) — Linear Elastic Fracture Mechanics (LEFM) Approach" 3 (1).

Jesus, Abílio M.P. De, Hernán Pinto, Alfonso Fernández-Canteli, Enrique Castillo, and José A.F.O. Correia. 2010. "Fatigue Assessment of a Riveted Shear Splice Based on a Probabilistic Model." *International Journal of Fatigue* 32 (2):453–62. https://doi.org/10.1016/j.ijfatigue.2009.09.004.

Kinloch, A. J., and R. J. Young. 1984. *Chapter 4 Shear Yielding*. *Fracture Behaviour of Polymers*. Vol. 2. https://doi.org/10.1016/0263-8223(84)90007-2.

Lakes, Roderic. 1998. *Viscoelastic Solids*. CRC Press.

———. 2009. *Viscoelastic Materials*. https://doi.org/10.1017/CBO9780511626722.

Lamela-Rey, Maria-Jesús, Alfonso Fernández-Canteli, Maria-Antonia Garcia-Prieto, Enrique Castillo-Ron, Enoc Sanz-Ablanedo, and Mónica García-Menéndez. 2007. "Probabilistic Design Model for Glazing Plates : A Standard Proposal for Building." *Glass Performance Days 2007*, 581–83. www.glassfiles.com.

Lamela, María Jesús, Alberto Ramos, Pelayo Fernández, Alfonso Fernández-Canteli, Constanze Przybilla, Consuelo Huerta, and Antonia Pacios. 2014. "Probabilistic Characterization of Glass under Different Type of Testing." *Procedia Materials Science* 3. Elsevier B.V.:2111–16. https://doi.org/10.1016/j.mspro.2014.06.341.

Leaderman, Herbert. 1941. "Elastic and Creep Properties of Filamentous Materials." Massachusetts Institute of Technology. http://hdl.handle.net/1721.1/45989.

Loidl, Dieter, Oskar Paris, H. Rennhofer, Martin Müller, and Herwig Peterlik. 2007. "Skin-Core Structure and Bimodal Weibull Distribution of the Strength of Carbon Fibers." *Carbon* 45 (14):2801–5. https://doi.org/10.1016/j.carbon.2007.09.011.

Muñiz-Calvente, Miguel, Alfonso Fernández Canteli, Valery Shlyannikov, and Enrique Castillo. 2015. "Probabilistic Weibull Methodology for Fracture Prediction of Brittle and Ductile Materials." *Applied Mechanics and Materials* 784 (2):443–51. https://doi.org/10.4028/www.scientific.net/AMM.784.443.

Pan, B., K. Qian, H. Xie, and A. Asundi. 2009. "Two-Dimensional Digital Image Correlation for in-Plane Displacement and Strain Measurement: A Review." *Meas Sci Technol* 20 (6):1–17.

Papazafeiropoulos, George, Miguel Muñiz-Calvente, and Emilio Martínez-Pañeda. 2017. "Abaqus2Matlab: A Suitable Tool for Finite Element Post-Processing." *Advances in*

Engineering Software 105. Elsevier Ltd:9–16. https://doi.org/10.1016/j.advengsoft.2017.01.006.

Press, William, Saul Teukolsky, William Vetterling, Brian Flannery, Eric Ziegel, William Press, Brian Flannery, Saul Teukolsky, and William Vetterling. 1987. *Numerical Recipes: The Art of Scientific Computing*. *Technometrics*. Vol. 29. https://doi.org/10.2307/1269484.

Przybilla, C. 2014. "Mechanical Characterization of Materials in Fracture and Fatigue Focussed on the Size Effect," no. September.

Przybilla, Constanze, Alfonso Fernández-Canteli, and Enrique Castillo. 2011. "Deriving the Primary Cumulative Distribution Function of Fracture Stress for Brittle Materials from 3- and 4-Point Bending Tests." *Journal of the European Ceramic Society* 31 (4):451–60. https://doi.org/10.1016/j.jeurceramsoc.2010.11.007.

———. 2013. "Maximum Likelihood Estimation for the Three-Parameter Weibull Cdf of Strength in Presence of Concurrent Flaw Populations." *Journal of the European Ceramic Society* 33 (10):1721–27. https://doi.org/10.1016/j.jeurceramsoc.2013.02.028.

Ryu, Hyo Sub, Young Hyun Joo, Sun Ok Kim, Kyoung Chan Park, and Sang Woong Youn. 2008. "Influence of Age and Regional Differences on Skin Elasticity as Measured by the Cutometer®." *Skin Research and Technology* 14 (3):354–58. https://doi.org/10.1111/j.1600-0846.2008.00302.x.

Salazar, A., P. M. Frontini, and J. Rodríguez. 2014. "Determination of Fracture Toughness of Propylene Polymers at Different Operating Temperatures." *Engineering Fracture Mechanics* 126. Elsevier Ltd:87–107. https://doi.org/10.1016/j.engfracmech.2014.04.023.

Schwarzl, F., and A. J. Staverman. 1952. "Time-Temperature Dependence of Linear Viscoelastic Behavior." *Journal of Applied Physics* 23:838.

Sutton, Michael A. 2008. "Digital Image Correlation for Shape and Deformation Measurements." In *Handbook of Experimental Solid Mechanics*, edited by William Sharpe Jr., 565–600. Springer US.

Tzikang, Chen. 2000. "Determining a Prony Series for a Viscoelastic Material From Time Varying Strain Data." *U.S. Army Research Laboratory Vehicle Technology Directorate Langley Research Center, Hampton, Virginia*, no. May:26.

Wang, Zhen, and Yuanming Xia. 1998. "Experimental Evaluation of the Strength Distribution of Fibers under High Strain Rates by Bimodal Weibull Distribution." *Composites Science and Technology* 57 (12):1599–1607. https://doi.org/10.1016/S0266-3538(97)00092-4.

Weibull, W. 1939. "A Statistical Theory of the Strength of Materials." *Ingeniorsvetenskapsakademiens*.

———. 1951. "A Statistical Distribution Function of Wide Applicability." *Journal of Applied Mechanics*. https://doi.org/citeulike-article-id:8491543.

Weil, N. A., and I. M. Daniel. 1964. "Analysis of Fracture Probabilities in Nonuniformly Stressed Brittle Materials." *Journal of the American Ceramic Society* 47 (6):268–74. https://doi.org/10.1111/j.1151-2916.1964.tb14413.x.

Williams, Malcolm L., Robert F. Landel, and John D. Ferry. 1955. "The Temperature Dependence of Relaxation Mechanisms in Amorphous Polymers and Other Glass-Forming Liquids." *Journal of the American Chemical Society* 77 (14):3701–7. https://doi.org/10.1021/ja01619a008.

Xia, L., and C. F. Shih. 1996. "Ductile Crack Growth-III. Transition to Cleavage Fracture Incorporating Statistics." *Journal of the Mechanics and Physics of Solids* 44:603–39.

APPENDIX A: EPOLAM 2025 – DATA SHEET

Axson TECHNOLOGIES

EPOLAM 2025

LAMINATING EPOXY RESIN

Tg 135°C

DESCRIPTION

EPOLAM 2025/2027 is formulated for structural composite applications, where thick sections are required with high temperature resistance.

PROPERTIES

- *Good chemical resistance*
- *Without aromatic amines*
- *High temperature resistance*
- *Good wetting reinforcements and fillers*
- *Low exotherm risk and long pot-life*
- *Thick laminated possible*

PHYSICAL PROPERTIES				
Composition		**RESIN**	**HARDENER**	**MIXED**
Mix ratio by weight Mix ratio by volume at 25°C		100 100	28 36	
Aspect		liquid	liquid	liquid
Colour		off-white	blue	light blue
Viscosity at 25°C (mPa.s)	BROOKFIELD LVT	6,000	18	1,300
Specific gravity at 25°C Specific gravity of cured product at 23°C	ISO 1675 : 1985 ISO 2781 : 1996	1.19 -	0.92 -	- 1.12
Pot life at 25°C on 500 g (min)	Gel Timer TECAM			60

MECHANICAL PROPERTIES at 23°C (1)			
Flexural modulus	ISO 178 :2001	MPa	3,200
Flexural strength	ISO 178 :2001	MPa	110
Tensile strength	ISO 527 :1993	MPa	56
Hardness	ISO 868 :2003	Shore D1	87
Glass transition temperature (Tg)	ISO 11359 : 2002	°C	135
Coefficient of thermal expansion	ISO 11359 : 1999	10^{-6} K^{-1}	85
Demoulding time at 25°C	-	h	24
Hardening time at 25°C	-	d	5
Gelation time @ 23°C on laminate *(5 plies / glass fabric 290 g/m²)* *(10 plies / glass fabric 290 g/m²)*	LT 051 : 1998	hr	4h10 3h50

N B : The above values were obtained with an neat resin (no reinforcement).

** The above properties, obtained using standard specimens and in precise chemical cross-linking conditions, represent the optimum values for this system after thermal treatment and complete cure (see processing conditions paragraph).*

Axson TECHNOLOGIES

EPOLAM 2025

LAMINATING EPOXY RESIN

Tg 135°C

PROCESSING CONDITIONS

After mixing according to the indicated ratio, impregnate the reinforcement according to the laminating process.

After 24 hours at room temperature, demould and postcure to the following schedule with a temperature gradient of 30°C/hr: 2 hr at 40°C, 2 hr at 60°C, 2 hr at 80°C, 2 hr at 100°C and 3 hr at 120°C and then a cool at maximum rate of 30°C/hr (which makes a global curing time of 14 hr)

If postcuring is carried out on a "concrete" mix comprising EPOLAM 2025 + aluminium granulate, it is best to double, or even triple, the duration at these plateau temperatures in order to ensure good heating throughout.

For an aluminium mix, use 120 to 150 gr of resin + hardener mix of EPOLAM 2025 per 500 gr of RZ 1019 granulate + 500 gr of RZ 1021 granulate. Mix the whole together using a planetary agitator and tamp down on to the laminate.

HANDLING PRECAUTIONS

Normal health and safety precautions should be observed when handling these products :

- *Ensure good ventilation*
- *Wear gloves, safety glasses and waterproof clothe.*

For further information, please consult the product safety data sheet.

STORAGE CONDITIONS

Shelf life is 24 months in a dry place and in original unopened containers at a temperature between 15 and 25°C. Any open must be tightly closed under dry nitrogen blanket.

PACKAGING

RESIN	***HARDENER***
1 x 5 kg *1 x 20 kg* *1 x 50 kg*	*1 x 1,4 kg* *1 x 5,6 kg* *1 x 14 kg* *1 x 180 kg*

GUARANTEE

The information of our technical data sheet are based on our present knowledge and the result of tests conducted under precise conditions. It is the responsibility of the user to determine the suitability of AXSON products, under their own conditions before commencing with the proposed application. AXSON refuse any guarantee about the compatibility of a product with any particular application. AXSON disclaim all responsibility for damage from any incident which results from the use of these products. The guarantee conditions are regulated by our general sale conditions.

APPENDIX B: ARAMIS' specifications

Project and Calibration Information

Calibration - Information

Calibration Date	Mon Dec 18 19:35:25 2017
Camera Lenses	50 mm
Calibration Temperature	22 °C
Calibration Object Type	Panel (coded)
Calibration Object	30x24 (50mm)

Calibration - Results

Calibration Deviation	0.032 pixel
Scale Deviation	0.000 mm
Camera Angle	24.9 deg
Measurement Volume	
Width:	37.5 mm
Height:	31.2 mm
Depth:	16.8 mm

Project - Information

Project Calculation Mode	Linear Strain
Facet Mode	Quadrangle Field
Facet Size (X x Y)	19 x 19
Facet Step (X x Y)	15 x 15
Number of Facets (X x Y)	162 x 136

Stage - Information

Stage 0	
Avg. Intersection Deviation	0.147 pixel
Max. Intersection Deviation	0.300 pixel

Image - Information

Image Width	2448 pixel
Image Height	2050 pixel

ARAMIS gom www.gom.com

APPENDIX C: ARAMIS data for specimen E22-7

Longitudinal strain [%]	Transversal strain [%]	Load [N]	Stress [Mpa]
0	0	3	0.1
0	0.02	2	0.1
0	0.01	3	0.1
0.05	0.01	36	1.4
0.12	-0.04	109	4.4
0.20	-0.07	170	6.8
0.28	-0.09	233	9.3
0.36	-0.12	304	12.1
0.47	-0.17	377	15.1
0.57	-0.22	456	18.2
0.67	-0.25	530	21.2
0.77	-0.29	605	24.2
0.87	-0.31	675	27.0
0.97	-0.36	744	29.8
1.08	-0.39	810	32.4
1.18	-0.43	876	35.0
1.28	-0.47	938	37.5
1.39	-0.52	999	40.0
1.48	-0.56	1056	42.2
1.58	-0.58	1111	44.4
1.67	-0.62	1166	46.6
1.77	-0.66	1218	48.7
1.86	-0.70	1268	50.7
1.97	-0.72	1319	52.8
2.07	-0.77	1366	54.6
2.17	-0.80	1416	56.6
2.29	-0.85	1463	58.5
2.42	-0.89	1516	60.7
2.54	-0.93	1568	62.7
2.68	-1.00	1621	64.8
2.80	-1.06	1665	66.6
2.94	-1.10	1711	68.5
3.08	-1.15	1755	70.2
3.22	-1.21	1797	71.9
3.36	-1.26	1833	73.3
3.50	-1.31	1869	74.8
3.65	-1.38	1901	76.0
3.79	-1.42	1929	77.2
3.96	-1.49	1961	78.4
4.11	-1.54	1993	79.7
4.27	-1.62	2016	80.6
4.44	-1.67	2042	81.7
4.60	-1.73	2066	82.6
4.78	-1.81	2083	83.3
4.95	-1.89	2103	84.1
5.12	-1.95	2122	84.9

APPENDIX D: Plastic data considered for the numerical model

Maximum stres	Plastic strain
30.03	0
31.57	2.55E-06
33.10	8.10E-06
34.60	6.86E-05
36.13	1.22E-04
37.59	1.94E-04
39.14	2.40E-04
40.60	3.15E-04
42.09	4.28E-04
43.54	5.02E-04
44.95	5.92E-04
46.38	7.25E-04
47.75	8.25E-04
49.09	9.85E-04
50.44	1.09E-03
51.73	1.27E-03
53.00	1.40E-03
54.27	1.58E-03
55.49	1.73E-03
56.71	1.92E-03
57.88	2.13E-03
59.04	2.35E-03
60.17	2.57E-03
61.29	2.75E-03
62.39	2.99E-03
63.43	3.24E-03
64.43	3.50E-03
65.43	3.77E-03
66.37	4.05E-03
67.30	4.28E-03
68.18	4.59E-03
69.01	4.85E-03
69.81	5.13E-03
70.52	5.44E-03
71.19	5.71E-03
71.76	6.02E-03
72.22	6.25E-03
72.70	6.49E-03
73.24	6.80E-03
73.90	7.07E-03
74.62	7.42E-03
75.35	7.77E-03
76.08	8.12E-03
76.78	8.47E-03
77.48	8.83E-03
78.14	9.24E-03
78.79	9.62E-03
79.42	1.00E-02
80.01	1.04E-02
80.59	1.09E-02
81.18	1.13E-02
81.73	1.17E-02
82.31	1.21E-02
82.84	1.26E-02
83.42	1.31E-02
83.97	1.36E-02
84.56	1.41E-02
85.20	1.46E-02
85.85	1.51E-02
86.50	1.57E-02
87.11	1.64E-02
87.71	1.70E-02
88.29	1.76E-02
88.82	1.82E-02
89.37	1.89E-02
89.88	1.97E-02
90.39	2.04E-02
90.89	2.11E-02
91.36	2.19E-02
91.82	2.27E-02
92.25	2.34E-02
92.65	2.42E-02

APPENDIX E: EFCDF, PFCDF and linear regression assuming $\lambda \geq 0$

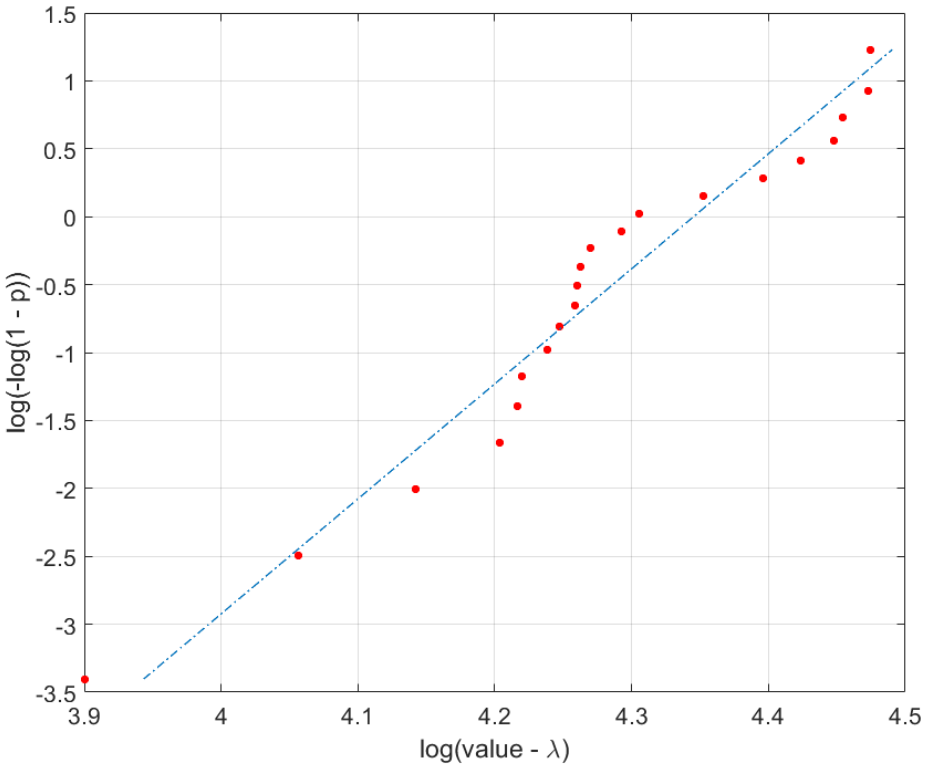

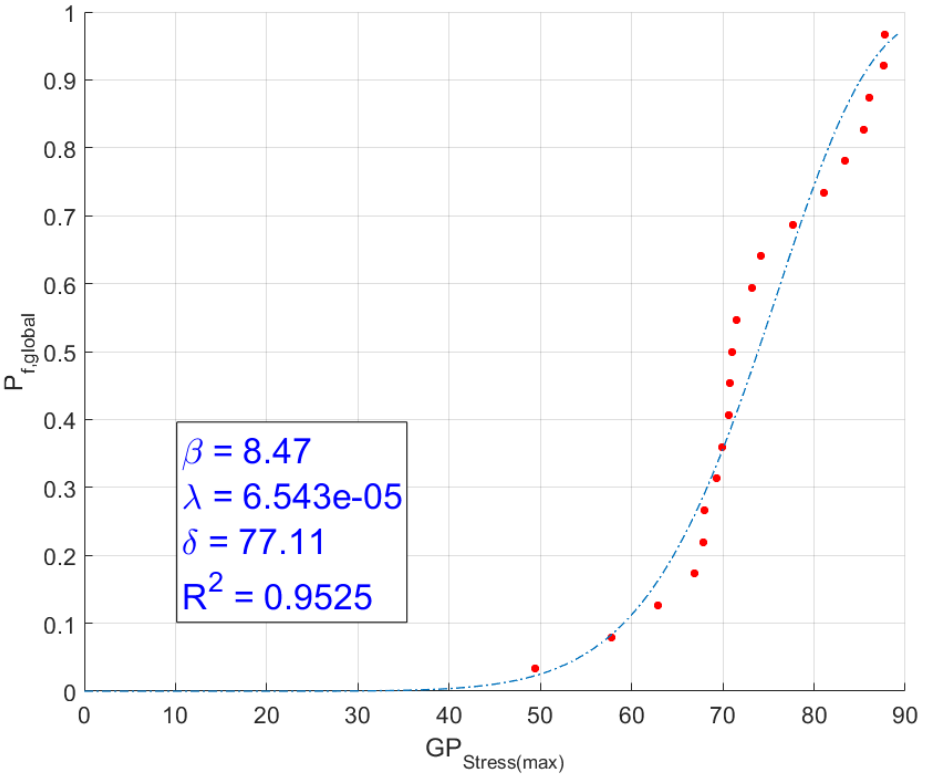

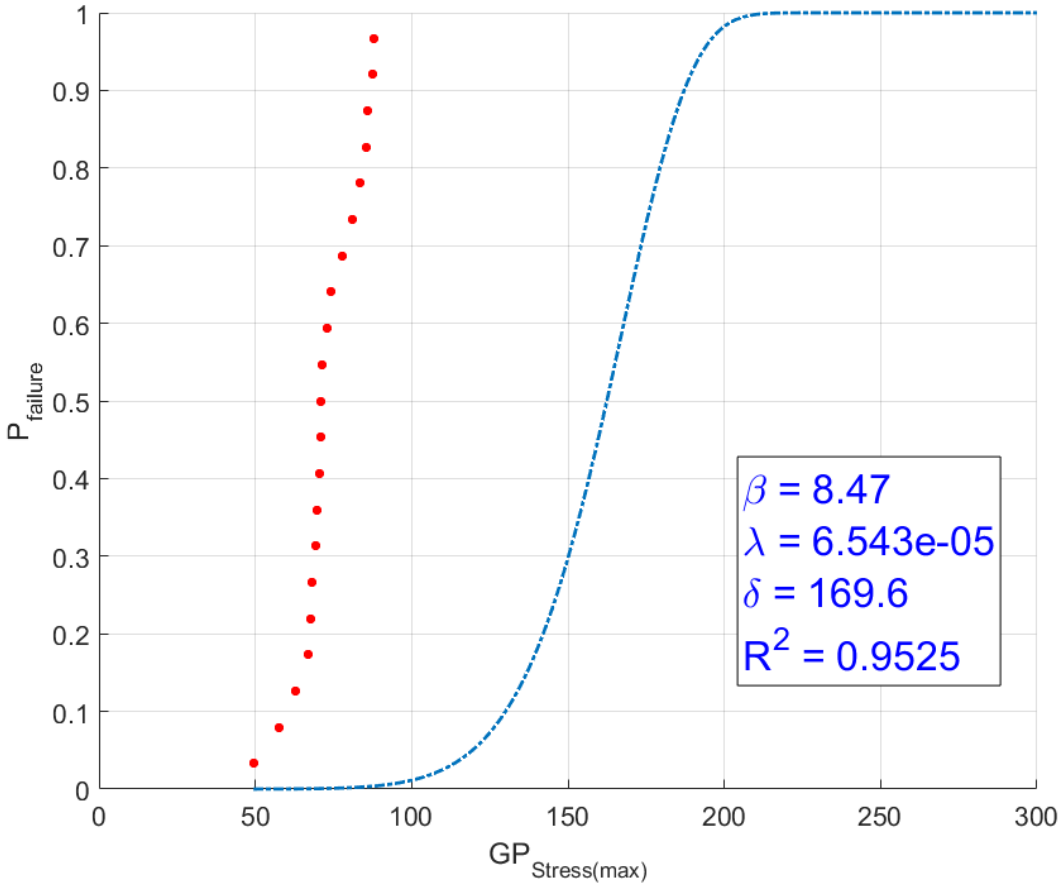
1
0.9
0.8
0.7
0.6
0.5
0.4
0.3
0.2
0.1
0
P failure
0
50
100
150
200
250
300
GP Stress(max)
β = 8.47
λ = 6.543e-05
δ = 169.6
R2 = 0.9525